A COMPARATIVE STUDY ON PRACTICAL MODELING OF STEEL I-GIRDER BRIDGES CONSIDERING RESTRAINED WARPING BEHAVIOR

A THESIS SUBMITTED TO
THE GRADUATE SCHOOL OF NATURAL AND APPLIED SCIENCES
OF
MIDDLE EAST TECHNICAL UNIVERSITY

BY

AYNUR ŞEYMA BULDUK

IN PARTIAL FULFILLMENT OF THE REQUIREMENTS
FOR
THE DEGREE OF MASTER OF SCIENCE
IN
CIVIL ENGINEERING

SEPTEMBER 2020

Approval of the thesis:

A COMPARATIVE STUDY ON PRACTICAL MODELING OF STEEL I-GIRDER BRIDGES CONSIDERING RESTRAINED WARPING BEHAVIOR

submitted by **AYNUR ŞEYMA BULDUK** in partial fulfillment of the requirements for the degree of **Master of Science in Civil Engineering, Middle East Technical University** by,

Prof. Dr. Halil Kalıpçılar
Dean, Graduate School of **Natural and Applied Sciences** _____

Prof. Dr. Ahmet Türer
Head of the Department, **Civil Engineering** _____

Prof. Dr. Özgür Kurç
Supervisor, **Civil Engineering, METU** _____

Examining Committee Members:

Prof. Dr. Cem Topkaya
Civil Engineering, METU _____

Prof. Dr. Özgür Kurç
Civil Engineering, METU _____

Prof. Dr. Yalın Arıcı
Civil Engineering, METU _____

Assoc. Prof. Dr. Ozan Cem Çelik
Civil Engineering, METU _____

Assoc. Prof. Dr. Alper Aldemir
Civil Engineering, Hacettepe Uni. _____

Date: 23.09.2020

I hereby declare that all information in this document has been obtained and presented in accordance with academic rules and ethical conduct. I also declare that, as required by these rules and conduct, I have fully cited and referenced all material and results that are not original to this work.

Name, Last name : Aynur Şeyma Bulduk

Signature :

ABSTRACT

A COMPARATIVE STUDY ON PRACTICAL MODELING OF STEEL I-GIRDER BRIDGES CONSIDERING RESTRAINED WARPING BEHAVIOR

Bulduk, Aynur Şeyma
Master of Science, Civil Engineering
Supervisor: Prof. Dr. Özgür Kurç

September 2020, 94 pages

Skewed and horizontally-curved steel I-girder bridges show complicated behavior due to the torsional action they exhibit under standard bridge loads, particularly during construction. The restrained warping response of girders can play a critical role in the analysis and design of these structures. In finite element analysis, the restrained warping behavior of girder can be considered through detailed 3D shell models or alternative methods such as utilizing an effective torsion constant in the analysis with conventional beam elements. However, there is still a need for an intermediate modeling approach for practical purposes, that is time-saving, reliable, and will provide specific analysis output parameters with sufficient accuracy. This study investigates different modeling approaches involving shell elements, beam elements with warping behavior, and the combination of shell-beam elements. Then, it evaluates to what extent a modeling approach that utilizes beam elements with an additional warping degree of freedom can produce accurate results compared to the other modeling approaches. For this purpose, a 3D frame analysis program is developed in MATLAB and different beam element formulations are implemented

into the program. Under construction loads, a straight I-girder, a horizontally-curved I-girder, and a horizontally-curved I-girder bridge are analyzed through the frame analysis program. Equivalent 3D shell models are constructed and analyzed in LARSA 4D finite element analysis software. The accuracy of twist angles, vertical deflections, major-axis and lateral bending moments, associated stresses, and cross-frame forces are discussed in a comparative manner. The main conclusion drawn from this study is that the beam element with an additional warping degree of freedom is capable of producing essential analysis output parameters with sufficient accuracy. Moreover, using shell and beam elements for modeling the web and flanges of an I-section, respectively, can be considered as an alternative and practical way of modeling such bridges.

Keywords: Constructibility, Curved Bridge, Finite Element Modeling, Restrained Warping, Steel I-girder

ÖZ

ÇELİK I-KİRİŞLİ KÖPRÜLERİN SINIRLANDIRILMIŞ ÇARPILMA DAVRANIŞI DİKKATE ALINARAK PRATİK MODELLENMESİ ÜZERİNE KARŞILAŞTIRMALI BİR ÇALIŞMA

Bulduk, Aynur Şeyma
Yüksek Lisans, İnşaat Mühendisliği
Tez Yöneticisi: Prof. Dr. Özgür Kurç

Eylül 2020, 94 sayfa

Eğik ve yatay kavisli çelik I-kiriş köprüler, özellikle inşaat sırasında standart köprü yükleri altında gösterdikleri burulma hareketi nedeniyle karmaşık bir davranışa sahiptirler. Kirişlerin sınırlandırılmış çarpılma tepkisi, bu yapıların analizi ve tasarımında kritik bir rol oynayabilir. Sonlu eleman analizinde, kirişin sınırlandırılmış çarpılma davranışı, detaylı üç boyutlu kabuk modelleri veya geleneksel kiriş elemanları ile birlikte analizde etkili bir burulma sabitinin kullanılması gibi alternatif yöntemlerle dikkate alınabilir. Bununla birlikte, pratik amaçlar için, zaman kazandıran, güvenilir ve belirli analiz çıktı parametrelerini yeterli doğrulukla sağlayacak bir ara modelleme yaklaşımına hala ihtiyaç vardır. Bu çalışma, kabuk elemanlarını, çarpılma davranışına sahip kiriş elemanlarını ve kabuk-kiriş elemanlarının kombinasyonunu içeren farklı modelleme yaklaşımlarını incelemektedir. Ayrıca, ek bir çarpılma serbestlik derecesine sahip kiriş elemanlarını kullanan modelleme yaklaşımının, belirtilen diğer modelleme yaklaşımlarına kıyasla ne kadar doğru sonuçlar üretebileceğini de değerlendirmektedir. Bu amaçla MATLAB'da üç boyutlu bir çerçeve analiz programı geliştirilmiş ve programa çeşitli

kiriş eleman formülasyonları entegre edilmiştir. İnşaat yükleri altında, düz bir I-kiriş, yatay kavisli bir I-kiriş ve yatay kavisli bir I-kiriş köprü, çerçeve analiz programı aracılığıyla çözümlenmiştir. Bunlara ek olarak, eşdeğer üç boyutlu kabuk modelleri, LARSA 4D programında oluşturulup çözümlenmiştir. Gerçekleştirilen bütün çözümlemeler sonrasında burulma açılarının, dikey sapmaların, ana eksen ve yanal eğilme momentlerinin ve ilişkili gerilmelerin, çapraz çerçeve kuvvetlerinin doğruluğu karşılaştırılmıştır. Sonuç olarak, çarpılma serbestlik derecesine sahip kiriş elemanının gerekli çözümleme sonuçlarını yeterli doğrulukta üretebildiği görülmüştür. Buna ek olarak, bir I-kesitin gövde ve flanşlarını modellemek için sırasıyla kabuk ve kiriş elemanlarının kullanılması bu tür köprüleri modellemede alternatif ve pratik bir yol olarak düşünülebilir.

Anahtar Kelimeler: Çelik I-kiriş, İnşa Edilebilirlik, Kavisli Köprü, Sınırlandırılmış Çarpılma, Sonlu Eleman Modellemesi

To My Family

ACKNOWLEDGEMENTS

I wish to express my deepest gratitude to my supervisor Prof. Dr. Özgür Kurç, for his guidance, advice, criticism, encouragement, and insight throughout the research.

I would like to express my deep and sincere gratitude to my family for their continuous love and support. I am grateful to my sister Elif Bulduk for always being there for me. I am thankful to my parents Serpil Bulduk and Tamer Bulduk, for giving me the opportunities and experiences that have made me who I am.

TABLE OF CONTENTS

LIST OF TABLES

TABLES

LIST OF FIGURES

FIGURES

CHAPTER 1

INTRODUCTION

In highway bridge construction, skewed and horizontally-curved bridges are preferred options in the presence of geometric restrictions, especially in the urban areas. In addition, steel I-section girders are preferred by engineers due to their economic advantages and ease of erection. In spite of their extensive usage, the behavior of these types of bridges is still not completely understood. Compared to non-skewed straight bridges, such bridges have more complicated behavior, which results from the torsional action that they exhibit under standard bridge loads, particularly during construction.

Under torsional loading, members with I-section warp in addition to twisting where warping takes place by lateral bending of the flanges. As shown in Figure 1-1, when the flanges of member ends are free to deform, the member undergoes homogeneous torsion, meaning that the applied torsion is entirely resisted by the St. Venant torsion. As shown in Figure 1-2, when the flanges of member ends are restrained, the member undergoes non-homogeneous torsion, i.e., the applied torsion is not only resisted by the St. Venant torsion but also by the warping torsion, implying that the additional normal and shear stresses develop in the flanges due to bending.

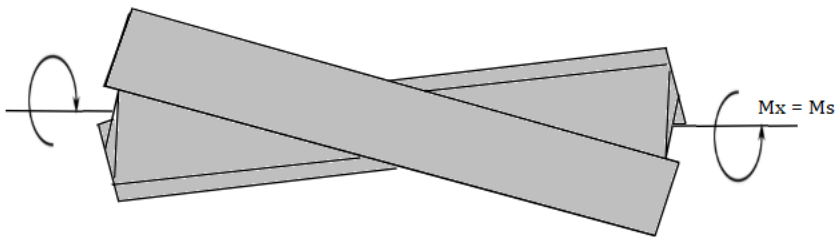

Figure 1-1 Homogeneous torsion in members with I-section.

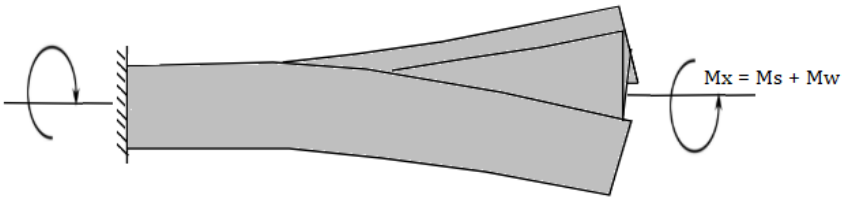

Figure 1-2 Non-homogeneous torsion in members with I-section.

For skewed and horizontally-curved steel I-girder bridges, the warping torsion can dominate the St. Venant torsion in the overall behavior of the structure. Besides, for all types of steel I-girder bridges with a concrete deck, the warping stiffness of girder can play a significant role in the torsional analysis of exterior girders under the eccentric loads acting on overhang forming brackets.

1.1 Problem Statement

The girder warping can be critical for both the analysis and design aspects of steel I-girder bridges. For skewed bridges, neglecting the girder warping stiffness limits the load transfer from cross-frames to girders and causes the cross-frame forces to be underestimated, which may lead to the insufficient design of cross-frame members. For horizontally-curved bridges, since bending and torsional actions are coupled, neglecting the girder warping stiffness may lead to errors in the prediction of major-axis bending response and corresponding stresses used in the design of girders. Likewise, in the torsional analysis of exterior girders, neglecting the girder warping stiffness causes the girder rotation to be overestimated; hence, the rotation limitations given by the design codes may not be satisfied. These are some of the examples emphasizing the need for considering the girder warping stiffness in the analysis and design of steel I-girder bridges.

In the finite element analysis of bridge superstructures, the effects of cross-section warping can be included in the analysis output through a refined finite element model by modeling the cross-section of I-girders with multiple shell elements. However, constructing such a model and interpreting analysis results may require specialized

knowledge of finite element method, additional computational cost, and can be time-consuming for practical purposes. Moreover, engineers are more familiar with the conventional beam element formulations, can easily interpret the analysis result, and directly use the analysis results in the design computations. Even though there are several beam element formulations that consider warping deformations, the accuracy and validity of such formulations are not well known, especially for steel I-girder bridges. Thus, the main focus of this study is to construct different structural models involving shell elements, beam elements with warping behavior, and the combination of shell-beam elements, compare the results, and propose a reliable, practical, and accurate way of considering the effect of warping for steel I-girder bridges.

1.2 Literature Review

In 1961, Vlasov developed a torsion theory for open section thin-walled beams considering the restrained warping. He introduced the concept of non-homogeneous torsion, the theory of sectorial areas, warping constant, and bi-moment. In order to consider the effect of restrained warping in the analysis and design, also to ease these processes, different approaches to the torsion problem of I-section members arose following the Vlasov's beam theory. One of these approaches was converting the torsion in the cross-section into a lateral force couple acting on the flanges and analyzing the warping of I-section member flanges analogous to the flexure problem. Based on the analytical solution, reduction factors for the obtained flange lateral bending moments were developed and tabulated to be used in the design for the simple, fixed and partial warping boundary conditions (Salmon, Johnson, & Malhas, 2009; Montoya-Vargas & Dario Aristizabal-Ochoa, 2019).

In finite element analysis through beam elements, the presence of an additional degree of freedom (DOF), which is the warping DOF, was considered by several researchers, and new element formulations with 14×14 stiffness matrices were developed. Barsoum and Gallagher (1970) studied the torsional and torsional-

flexural instability by introducing elastic and geometric stiffness matrices with the warping DOF. A polynomial approximation was used in the formulation. Waldron (1986) derived a member stiffness matrix with the warping DOF by inverting the appropriate member flexibility matrix and considering the equilibrium of member ends. Yang and McGuire (1984) introduced the warping spring concept to analyze partial warping restraint conditions. The stiffness matrix developed by Barsoum and Gallagher (1970) was employed in the study and a static condensation procedure was applied to eliminate the non-continuous warping DOF at the member ends with restrained warping.

In Vlasov's beam theory, the cross-section is assumed to be undeformable in its own plane, and shear deformation effects are neglected. Benscoter (1954), on the other hand, introduced a beam theory for thin-walled beams which incorporates shear deformations and characterizes warping as an independent function rather than considering it as the rate of change of twist angle. While the aforementioned element formulations are based on Vlasov's theory, there are other researchers in the literature (Shakourzadeh, Guo, & Batoz, 1995) who formulated the beam elements for both open and closed cross-sections based on Benscoter's theory.

Another study that was conducted by Ahmed and Weisgerber (1996) accounts for the warping of I-section members in the commercial software programs that employ conventional beam element formulations with a 6×6 stiffness matrix for grid or 12×12 stiffness matrix for space frame structural models. The torsional stiffness associated with homogeneous torsion was equated to the analytical torsional stiffness associated with non-homogeneous torsion and an effective torsion constant was developed. The effective torsion constant was defined for I-section members having warping fixity at both ends, warping fixity at one end and free warping at the other end, and partial warping restraint at both ends. The warping spring concept proposed by Yang and McGuire (1984) was adopted to analyze the partial warping boundary conditions.

In the literature, several other researchers have investigated the behavior of steel I-girder bridges through finite element analysis by modeling girders as beam elements. Either the element formulations with warping effects, some discussed in the preceding paragraphs, were employed or warping effects were included in the analysis by approximate methods. Zhang, Huang, and Wang (2005) conducted a parametric study to investigate the live load distribution of horizontally-curved I-girder bridges and developed equations for the live load distribution factors. The bridges were modeled as a generalized grillage beam system and thin-walled curved beam elements considering warping torsion were utilized in modeling girders. The generalized grillage model was compared with a detailed 3D finite element model for verification. Linzell and Shura (2010) worked on a large radius, horizontally-curved steel I-girder bridge, and presented the comparison of construction field data with the results of finite element grillage models simulating the actual construction sequence. The goal of the study was to assess the limitations of standard analysis methods that are extensively used by practicing engineers. Therefore, the conventional frame elements were employed to model girders and cross-frames, and the warping stresses were estimated by an approximate method, namely the V-load method. It was reported that the grillage models of the study combined with the V-load method produced poor results against the field data. Chang and White (2008) assessed the qualities and limitations of a number of finite element modeling considerations for composite curved steel I-girder bridges. The modeling requirements were emphasized for the composite section in which the deck slab either modeled by beam or shell elements, and girders modeled by beam elements considering the warping as an additional DOF. For modeling purposes, the commercial finite element analysis packages were used such as ABAQUS. It was concluded that the detailed 3D shell element models and 3D grid models with girder elements having warping DOF are the most accurate representations of the structural response.

Sanchez and White (2017) discussed the qualities and limitations of various finite element analysis methods for curved and skewed I-girder bridges as a part of efforts

under Project NCHRP 12-79 (White et al., 2012). The focus of the study was non-composite response during construction, emphasizing inaccuracies in the analysis through traditional 2D-grid models, and improvements were proposed to eliminate these inaccuracies. The approximate method suggested to include warping effects in the analysis was the use of effective torsion constants developed by Ahmed and Weisgerber (1996).

1.3 Objective and Scope

The main objective of this study is to compare the torsional responses of different modeling approaches used for modeling straight or curved steel I-girder bridges in terms of the accuracy of these approaches, their practical use, and feasibility of use in conventional finite element analysis software. A two-node warping beam element having seven DOF at each node will be developed by combining the stiffness matrix of the conventional two-node Timoshenko beam element with the 4×4 torsional stiffness matrix derived based on the Vlasov's beam theory. The element will be implemented into a frame analysis program, namely the 3D Frame Analysis Program, that will be coded in MATLAB, using the direct stiffness method for the analysis of frames in three-dimensional space. In addition to this element, conventional beam elements and the effective torsion concept proposed by Ahmed and Weisgerber (1996) will be included in the program. In all formulations, only linear elastic behavior will be considered. In addition to the finite element models constructed by beam elements, refined finite element models with shell elements and the combination of beam and shell elements will also be constructed and analyzed utilizing LARSA 4D finite element analysis software. Then, the results obtained from all structural models, which account for warping effects, will be compared with the analytical solution for validation purposes.

Case studies will be conducted by analyzing straight and curved girder models, and a horizontally-curved bridge model with girders and cross-frames. The case studies will focus on the non-composite response of girders under construction loads and

important design parameters such as major-axis bending stress and flange lateral bending stress. Only the results of the linear static analysis will be compared.

CHAPTER 2

BEAM ELEMENT FORMULATIONS AND IMPLEMENTATION OF 3D FRAME ANALYSIS PROGRAM

A new 3D Frame Analysis Program has been developed in MATLAB to analyze the structures that were investigated in this study using different beam formulations. The elements available in this program are the space truss, 6 DOF conventional beam, 6 DOF beam with effective torsion constant to consider warping effects, and a 7 DOF warping beam element, including warping behavior as an additional degree of freedom. The program can analyze members in which the cross-section's shear center and centroid coincide. In this study, the program was used to analyze such members with doubly-symmetric I-sections.

This chapter provides a theoretical background for the torsional analysis of steel I-section members, including the derivation of a 4×4 torsional stiffness matrix, and outlines the implementation of the program. All expressions given in derivation of the 4×4 torsional stiffness matrix are based on linear elastic behavior assumption.

2.1 Torsional Analysis of Steel I-Section Members

When members having a solid circular cross-section are subjected to torsion, twisting occurs about the member's longitudinal axis, and the cross-sections initially plane remain plane after twisting. On the contrary, when members having a non-circular cross-section are subjected to torsion, the applied torsion is resisted by both twisting and warping of the cross-section, and the cross-sections initially plane do not remain plane after deformations take place.

In the case of members with I-section, the applied torsion is resisted by the twisting of the whole cross-section and the warping of the flanges. For such members, the member internal torsion can be divided into two parts: the St. Venant torsion and the warping torsion. When flanges at the member ends are allowed to deform freely, the member undergoes homogeneous torsion, i.e., the applied torsion is entirely resisted by the St. Venant torsion. When flanges of the member ends are restrained, the member undergoes non-homogeneous torsion, i.e., the applied torsion is resisted by the St. Venant torsion and warping torsion. Thus, the torsional analysis of such sections should consider the warping torsion as well as the St. Venant torsion.

2.1.1 Sources of torsion

The torsion in the cross-section can either result from an externally applied torsional moment or an eccentrically applied transverse force. While the eccentricity of longitudinal forces causing flexural moments are measured relative to the geometric centroid of the cross-section, the eccentricity of transverse forces creating torsion is measured relative to the shear center of the cross-section. The shear center is a point in the cross-section through which the applied transverse forces do not produce torsion. As shown in Figure 2-1(a), for a single-symmetric I-section, the shear center lies on the axis of symmetry but does not coincide with the centroid. As shown in Figure 2-1(b), for a doubly-symmetric I-section, the shear center coincides with the centroid of the cross-section.

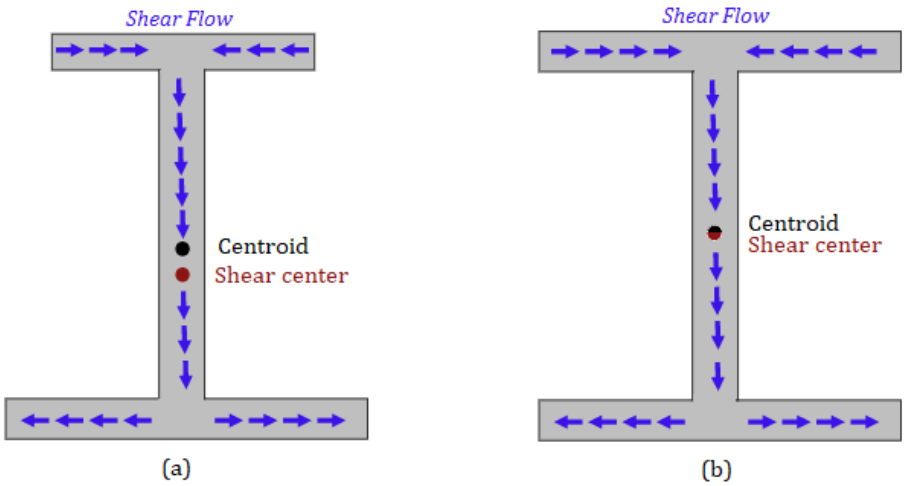

Figure 2-1 The centroid and shear center of an I-section: (a) Single-symmetric I-section; (b) Doubly-symmetric I-section.

2.1.2 St. Venant torsion, M_s

The St. Venant torsion (or pure torsion) component of the member internal torsion is calculated in the same way as the torsion of circular bars by assuming the member ends free to warp (Figure 2-2).

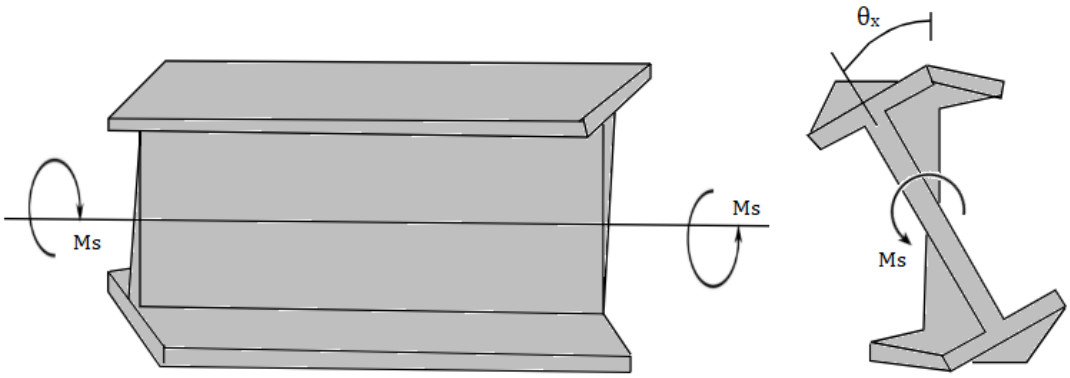

Figure 2-2 The St. Venant torsion (pure torsion).

Similar to the flexural curvature, the torsional curvature (or the rate of change of the angle of twist) is expressed as the moment divided by the torsional rigidity. The St. Venant torsion, M_s, is given by

$$M_s = GJ\frac{d\theta_x}{dx} \tag{2-1}$$

Where θ_x is the angle of twist, G is the shear modulus, and J is the torsion constant.

2.1.3 Warping torsion, M_w

When I-section members are subjected to torsion, the warping of the cross-section takes place through opposite in-plane flange rotations. In other words, the cross-section does not remain plane due to the lateral bending of flanges in opposite directions.

In the presence of a warping restraint, the normal stresses and shear stresses develop in the flanges, and the warping torsion component of the member internal torsion arises. Vlasov's theory considers restrained warping of thin-walled members by neglecting shear deformation effects and assuming that the web remains plane during twisting (Vlasov, 1961). In the torsional analysis of I-section members, the effect of secondary shear stresses on warping is negligible because these members have small torsional rigidity and exhibit large amounts of warping. Besides that, girders having thin webs are generally provided with stiffeners. Therefore, the assumptions of Vlasov's theory is admissible for practical purposes. Under the same premises, the expression for the warping torsion can be obtained by analyzing the lateral bending of the flanges.

Since the resulting action is torsion, the normal and shear stress developing in the flanges will be self-equilibrating. As shown in Figure 2-3, the flange lateral bending moments form a couple called bi-moment and associated flange shears in opposite directions form a couple which resists the applied torsion.

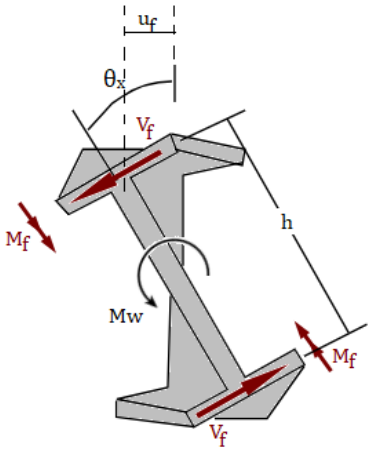

Figure 2-3 The warping torsion.

For small values of twist angle, the lateral displacement of one of the flanges is,

$$u_f = \theta_x \frac{h}{2} \tag{2-2}$$

where h is the distance between flange centroids.

The moment-curvature relationship for one flange is,

$$\frac{d^2 u_f}{dx^2} = -\frac{M_f}{EI_f} \tag{2-3}$$

where M_f is the lateral bending moment, E is the modulus of elasticity, and I_f is the associated moment of inertia for one flange.

Differentiating Equation 2-2 two times and inserting into Equation 2-3, the following relationship is obtained,

$$-\frac{M_f}{EI_f} = \left(\frac{h}{2}\right)\frac{d^2\theta_x}{dx^2} \tag{2-4}$$

Multiplying Equation 2-4 by the distance between flange centroids and rearranging the terms, the expression for the bi-moment, B, is obtained as

$$B = M_f h = -E\left[I_f\left(\frac{h^2}{2}\right)\right]\frac{d^2\theta_x}{dx^2} = -EC_w\frac{d^2\theta_x}{dx^2} \quad (2\text{-}5)$$

where C_w is the warping constant and equals to $I_f h^2/2$ for an I-section.

The shear force, V_f, in each flange is given by,

$$V_f = \frac{dM_f}{dx} \quad (2\text{-}6)$$

Differentiating Equation 2-3 and inserting Equation 2-6 into Equation 2-3, then differentiating Equation 2-2 three times, the following relationship is obtained:

$$\frac{d^3u_f}{dx^3} = -\frac{V_f}{EI_f} = \left(\frac{h}{2}\right)\frac{d^3\theta_x}{dx^3} \quad (2\text{-}7)$$

Finally, the expression for the warping torsion, M_w, is obtained by rearranging the terms of Equation 2-7:

$$M_w = V_f h = -E\left[I_f\left(\frac{h^2}{2}\right)\right]\frac{d^3\theta_x}{dx^3} = -EC_w\frac{d^3\theta_x}{dx^3} \quad (2\text{-}8)$$

2.1.4 Governing differential equation for torsional deformation

The governing differential equation for the torsional deformation can be written as the sum of the St. Venant torsion (Equation 2-1) and warping torsion (Equation 2-8),

$$M_x = M_s + M_w = GJ\frac{d\theta_x}{dx} - EC_w\frac{d^3\theta_x}{dx^3} \quad (2\text{-}9)$$

where M_x is the total torsional moment.

2.1.5 Stiffness matrix

In the construction of the stiffness matrix for torsional analysis of I-section members with restrained warping, the Principle of Virtual Work was applied. For the St. Venant torsion, the virtual work of the internal forces is given by

$$\partial W_{int,s} = \int_0^L \frac{d(\partial\theta_x)}{dx} M_s \, dx = \int_0^L \frac{d(\partial\theta_x)}{dx} GJ \frac{d(\theta_x)}{dx} \, dx \tag{2-10}$$

Likewise, the virtual work for the warping torsion can be computed by

$$\partial W_{int,w} = 2\int_0^L \frac{d^2(\partial u_f)}{dx^2} M_f \, dx = 2\int_0^L \frac{d^2(\partial\theta_x)}{dx^2} \frac{h}{2} \frac{EC_w}{h} \frac{d^2(\theta_x)}{dx^2} \, dx$$

$$\partial W_{int,w} = \int_0^L \frac{d(\partial\theta'_x)}{dx} EC_w \frac{d(\theta'_x)}{dx} \, dx \tag{2-11}$$

The external work done by the applied forces is equal to

$$\partial W_{ext} = [\partial\theta_x]\{M_x\} + [\partial\theta'_x]\{B\} \tag{2-12}$$

Then, the torsional deformations can be applied by approximating the displacement field by the appropriate shape functions, [N] = [N_1 N_2 N_3 N_4]:

$$\partial W_{int,s} + \partial W_{int,w} = \partial W_{ext}$$

$$[\partial\theta_x]\left[\int_0^L [N']^T GJ[N']dx\right]\{\theta_x\} + [\partial\theta'_x]\left[\int_0^L [N'']^T EC_w[N'']dx\right]\{\theta'_x\}$$

$$= [\partial\theta_x]\{M_x\} + [\partial\theta'_x]\{B\} \tag{2-13}$$

The corresponding stiffness matrix can be expressed as follows:

$$[k] = \left[\int_0^L [N']^T GJ[N']dx + \int_0^L [N'']^T EC_w[N'']dx\right] \tag{2-14}$$

Similar to the flexure problem, the displacement field was approximated by shape functions that provide C^1 interelement continuity, the simplest shape functions which satisfy the continuity of displacement and slope: Hermitian cubic shape functions.

Therefore, with Hermitian cubic shape functions, the stiffness matrix can be computed as:

$$[k] = \frac{E}{L^3}\begin{bmatrix} \frac{6GJL^2}{5E} & -\frac{6GJL^2}{5E} & \frac{GJL^3}{10E} & \frac{GJL^3}{10E} \\ & \frac{6GJL^2}{5E} & -\frac{GJL^3}{10E} & -\frac{GJL^3}{10E} \\ Sym. & & \frac{2GJL^4}{15E} & -\frac{GJL^4}{30E} \\ & & & \frac{2GJL^4}{15E} \end{bmatrix}$$

$$+\frac{E}{L^3}\begin{bmatrix} 12C_w & -12C_w & 6C_wL & 6C_wL \\ & 12C_w & -6C_wL & -6C_wL \\ Sym. & & 4C_wL^2 & 2C_wL^2 \\ & & & 4C_wL^2 \end{bmatrix}$$

2.2 Implementation of the Analysis Program

The program consists of a MATLAB code that performs the structural analysis and two Microsoft Excel workbooks that are used to take inputs and write outputs. The input spreadsheets are organized to take information regarding the joints, members, support, and loading conditions of the analysis model. The output spreadsheets are organized to report joint displacements, member forces, and support reactions. The format of input and output spreadsheets and detailed explanations of input and output data are provided in Appendix B.

In the subsequent sections, the algorithm of the program and the formulation of the element stiffness matrices available in the program are summarized.

2.2.1 Algorithm of the program

The main structure of the algorithm is shown in Figure 2-4. The program starts by reading input data and storing data of each input spreadsheet in matrix form. Next, the analysis model's active degrees of freedom are labeled according to the support conditions. Then, the global structural stiffness matrix is assembled after constructing the element stiffness matrix and transforming it from local coordinates to global coordinates for each element.

In 3D coordinate transformation, the warping DOF for the rate of twist is treated as a scalar quantity associated with the cross-sectional deformation; therefore, it is not transformed (Damkilde, 1999).

Following the assembly of the structural stiffness matrix, the force vector is formed by combining the nodal forces with fixed end forces obtained from the member loads available in the program. In the element force recovery, the uniform torsion load is directly distributed to nodes as concentrated torques, and the bi-moment is only treated as a nodal load imposed in the direction of warping DOF.

After obtaining the structural stiffness matrix, K, and corresponding force vector, F, the program solves the stiffness relationship given by Equation 2-15 to determine the joint displacement vector, d:

$$[F] = [K][d] \tag{2-15}$$

The program continues with post-processing joint displacements to compute member end forces and support reactions. As a final step, the outputs of the program are written to an Excel workbook in separate spreadsheets.

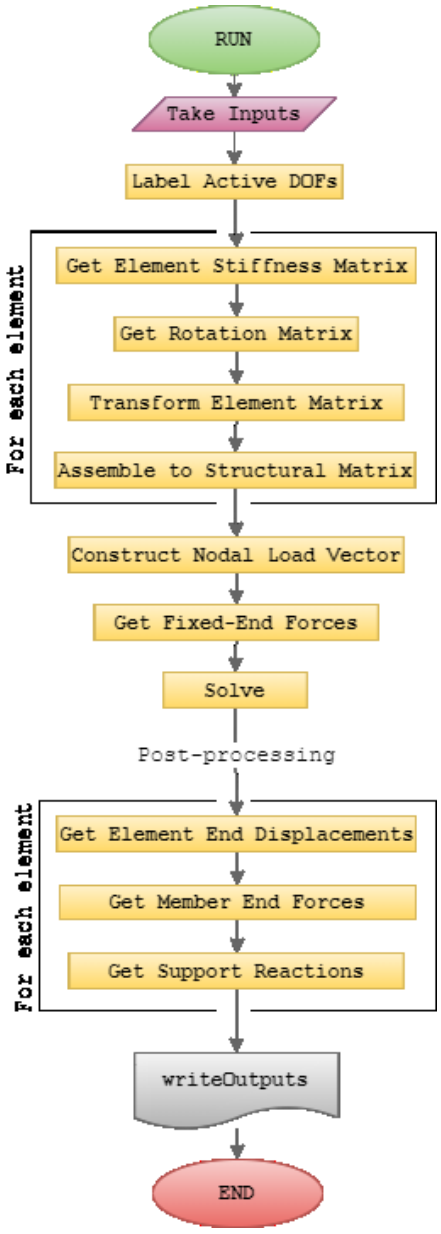

Figure 2-4 Algorithm of the program.

2.2.2 Truss element

In order to model axial-load carrying members, a standard two-node space truss element is implemented into the program. The stiffness matrix for the element is provided in Appendix A.

2.2.3 6 DOF beam element

The conventional two-node Timoshenko beam element having six DOF per node is implemented into the program. The stiffness matrix for the element is provided in Appendix A.

2.2.4 6 DOF beam element with the effective torsion constant, J_{eff}

This element is an extension of the 6 DOF Beam Element. The element formulation includes an effective torsion constant to take into account warping deformation effects in I-section members. Two effective torsion constants are implemented into the program: one for the members having warping fixity at each end, another one for the members having warping fixity at one end and warping free boundary condition at the other end. The expressions for the corresponding effective torsion constants were derived by employing these boundary conditions in the general equation of torsional rotation, Equation 2-9 (Ahmed and Weisgerber, 1996).

The effective torsion constant for the element with warping fixity at both ends is calculated by

$$J_{eff} = J\left[1 - \frac{\sinh(kL_b)}{kL_b} + \frac{[\cosh(kL_b) - 1]^2}{kL_b \sinh(kL_b)}\right]^{-1} \quad (2\text{-}16)$$

whereas the effective torsion constant for the element with warping fixity at one end and warping free boundary condition at the other end is calculated by

$$J_{eff} = J\left[1 - \frac{\sinh(kL_b)}{kL_b \cosh(kL_b)}\right]^{-1} \quad (2\text{-}17)$$

where $k = \sqrt{GJ/EC_w}$, and L_b is the unbraced length corresponding to the distance between warping boundaries.

The stiffness matrix for this element is same as the 6 DOF Beam Element, except that the torsion constant is replaced by the effective torsion constant.

2.2.5 7 DOF warping beam element

This element is a two-node beam element, including warping behavior as an additional DOF and having seven DOF per node. The element formulated by Barsoum and Gallagher (1970) is employed in this study with the modified flexural stiffness terms to account for flexural shear deformations. The axial and flexural stiffness terms of the element stiffness matrix are same as the conventional Timoshenko beam element. The torsional stiffness terms of the element stiffness matrix are same as terms of the 4×4 stiffness matrix derived in Section 2.1.5. In parallel to the assumptions employed in the derivation of the 4×4 torsional stiffness matrix, the element neglects web distortion and the effect of shear deformations on warping. The complete stiffness matrix for the element is provided in Appendix A.

CHAPTER 3

VALIDATION OF DIFFERENT MODELING APPROACHES UNDER TORSION

In this chapter, different modeling approaches are validated by investigating the torsional response of a steel I-section member subjected to concentrated torsional moment. The member is analyzed under torsionally fixed-free and fixed-fixed boundary conditions through two verification problems.

The verification problems are analyzed in 3D Frame Analysis Program utilizing beam elements that account for warping effects. These are the 6 DOF conventional Timoshenko beam element with effective torsion constant and 7 DOF warping beam element. The verification problems are also modeled in LARSA 4D finite element analysis software with flat shell elements. In addition to refined full-shell finite element models in which multiple shell elements constitute the cross-section of the member, an alternative modeling approach is considered by modeling the web of the cross-section with shell elements and its flanges with beam elements.

The results obtained from refined models and beam models are compared with the analytical solution. The mesh size and shell element type of the validated shell model to be used in case studies are presented. The key output parameters used for verifying the analysis results are the twist angle θ_x, rate of twist θ'_x, St.Venant torsion M_s, warping torsion M_w, and bi-moment B.

3.1 Section and Material Properties

The cross-sectional dimensions of the example doubly-symmetric I-section are shown in Figure 3-1, and sectional and material properties used in the analysis of verification problems are presented in Table 3-1.

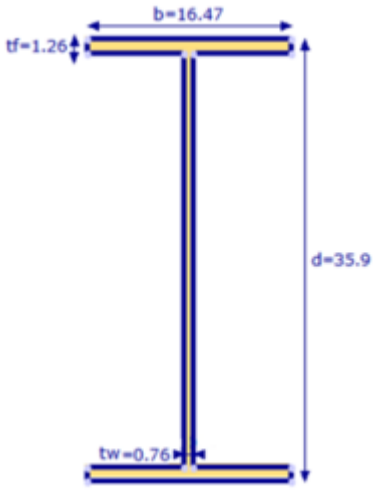

Depth (d) = 35.9 in

Flange width (b) = 16.47 in

Flange thickness (t_f) = 1.26 in

Web thickness (t_w) = 0.76 in

Figure 3-1 Cross-sectional dimensions of the example section.

Table 3-1 Sectional and material properties of the example section.

Cross-Sectional Properties	
Area (A)	66.87 in^2
Moment of inertia about the z-axis (I_z)	14811.6 in^4
Moment of inertia about the y-axis (I_y)	939.43 in^4
Torsion constant (J)	27.196 in^4
Warping constant (C_w)	281210 in^6
Material Properties	
Modulus of elasticity (E)	29000 ksi
Shear modulus (G)	11200 ksi

3.2 Verification Problem 1: Torsionally Fixed-Free Beam

The 15 ft long member having torsionally fixed-free boundary conditions was subjected to T = 100 kip-in concentrated torsional moment at the tip (Figure 3-2). The results of beam and shell models were compared with the analytical solution.

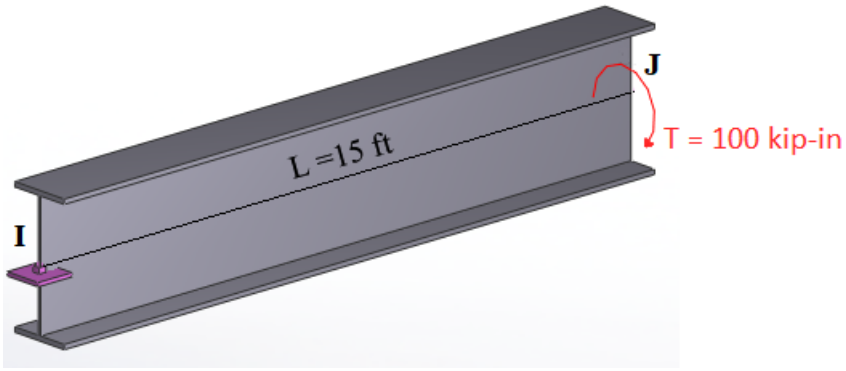

Figure 3-2 Geometry of Verification Problem 1.

3.2.1 Analytical solution

The boundary conditions of Verification Problem 1 dictate that the beam is not able to twist or warp at end I and free to warp at end J:

$$\theta_x(x) = 0 \text{ at } x = 0 \tag{3-1}$$

$$\theta'_x(x) = 0 \text{ at } x = 0 \tag{3-2}$$

$$B(x) = 0 \text{ or } \theta''_x(x) = 0 \text{ at } x = L \tag{3-3}$$

Solving the governing differential equation for torsional deformation, Equation 2-9, for this particular case results in:

$$\theta_x = \frac{T}{GJk}[\tanh kL * (\cosh kx - 1) - \sinh kx + kx] \tag{3-4}$$

where $k = \sqrt{GJ/EC_w}$. The parameters M_s, M_w, and B are obtained by taking derivatives of θ_x and inserting into expressions given by Equations 2-1, 2-8, 2-5, respectively.

3.2.2 Beam models

The verification problem was solved in 3D Frame Analysis Program by utilizing the 6 DOF beam elements with J_{eff} and 7 DOF warping beam elements.

Since the effective torsion constant is defined just for torsionally fixed-free and fixed-fixed connections for an element, a single beam element with J_{eff} was used to model the verification problem. The twist angle is the output parameter included in the reported results.

The twist angle, rate of twist, total torsion, and bi-moment are direct outputs of the program for the warping beam element. The St. Venant torsion is obtained using the rate of twist, and the warping torsion is obtained by subtracting the St.Venant torsion from the total torsion.

The results of the analytical solution and 3D Frame Analysis Program presented in Table 3-2 show that both beam formulations are capable of capturing the analytical solution even with a single beam element.

Table 3-2 Analysis results at the member ends.

	Analytical Solution	1 Beam Element with J_{eff}	1 Warping Beam Element	10 Warping Beam Elements
θ_x (rad) at x = L	0.01609	0.01609	0.01608	0.01609
M_s (kip-in) at x = L	40.07	-	40.01	40.07
M_w (kip-in) at x = L	59.93	-	59.99	59.93
B (kip-in^2) at x = 0	-13099	-	-13104	-13099

Figure 3-3 to Figure 3-6 show the variation of displacements and forces along the member for the analytical solution and warping beam elements. The analysis results extracted from intermediate elements are also in line with the analytical solution. At the fixed end, the total torsion is entirely carried by the warping torsion, and the bi-moment is at its maximum. Both warping torsion and bi-moment decrease towards the warping-free end of the member. At $x = L$, while the total torsion is shared by the St.Venant torsion, the bi-moment reaches zero.

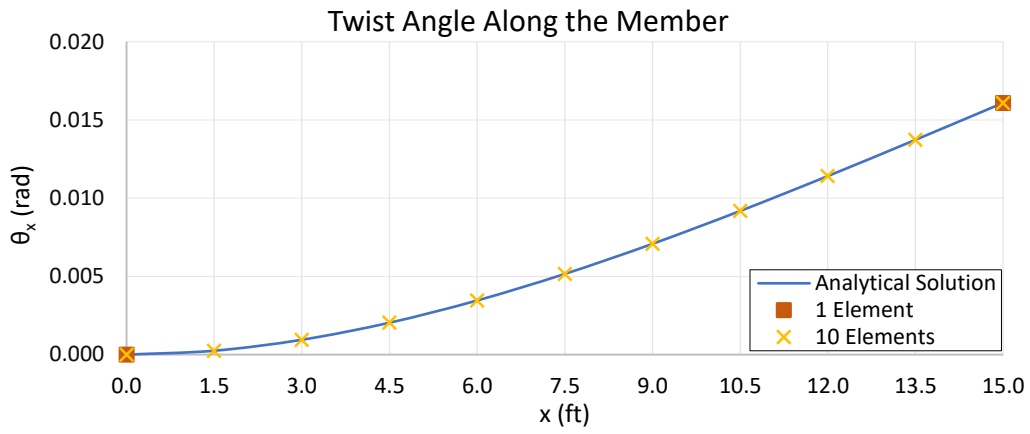

Figure 3-3 Verification Problem 1: Twist angle along the member.

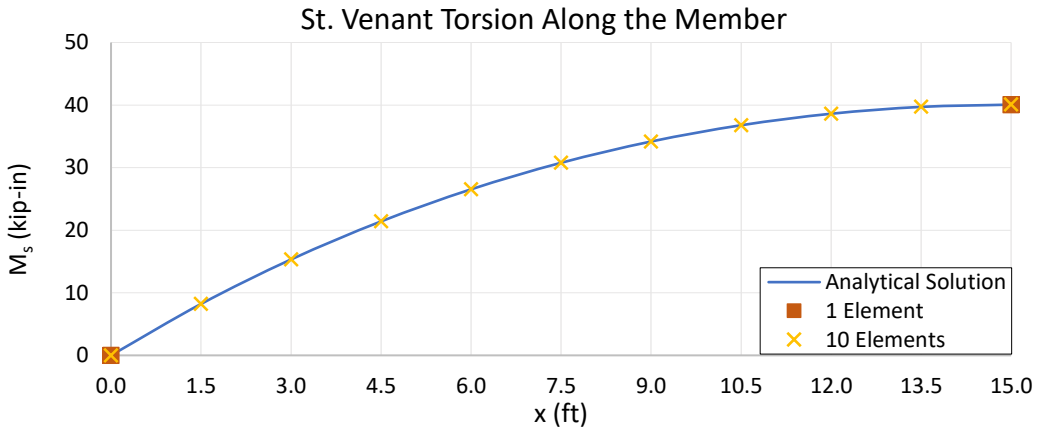

Figure 3-4 Verification Problem 1: St. Venant torsion along the member.

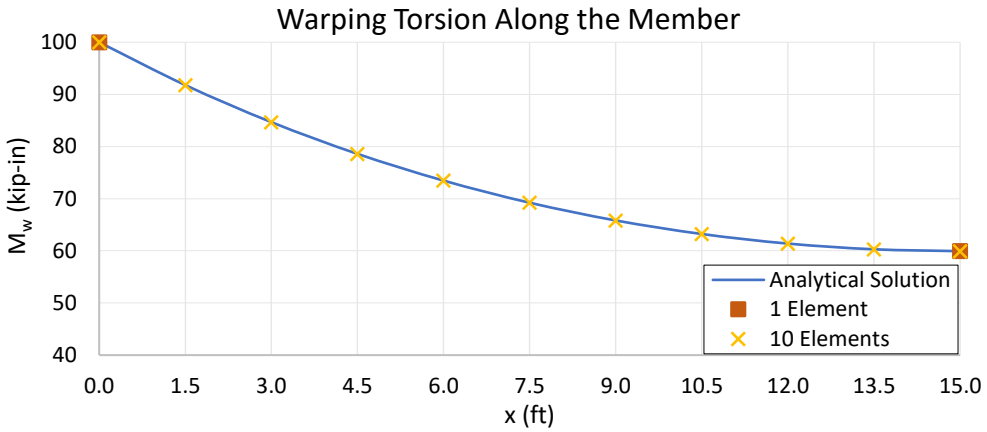

Figure 3-5 Verification Problem 1: Warping torsion along the member.

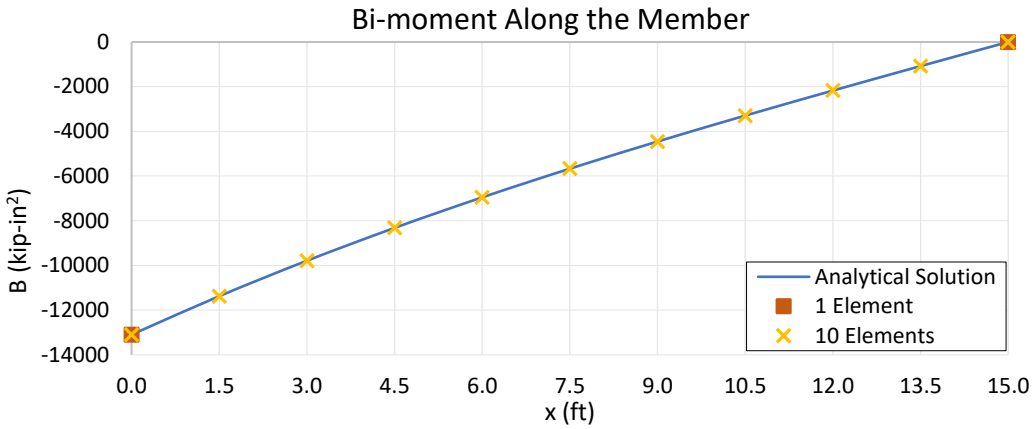

Figure 3-6 Verification Problem 1: Bi-moment along the member.

3.2.3 Shell models

The verification problem was modeled in LARSA 4D program with flat shell elements. First, full-shell models with different mesh sizes are constructed and analyzed. Then, the twist angles obtained from shell models are compared with the analytical solution. Next, the mesh size, element type, and detailed analysis results of the refined full-shell model, which is found adequate in producing accurate results, are presented together with the analytical solution. Finally, the detailed analysis results associated with the alternative modeling approach, in which the web of the cross-section is modeled with shell elements and its flanges with beam elements, are reported together with the analytical solution.

The thin plate element is employed in models, together with drilling and incompatible membranes. The details of the plate and membrane element formulations are as follows:

- *Thin plate:* The plate element based on Kirchoff Plate Theory, which assumes no transverse shear deformations through the element thickness. (Batoz & Tahar, 1982)

- *Incompatible membrane:* The membrane element with incompatible modes, which have a higher-order displacement definition to avoid shear locking that exists in the bilinear membrane. (Cook et al., 2001)
- *Drilling membrane:* The membrane element with quadratic displacement field definition and a rotational degree of freedom, which is defined from the displacement of the mid-points of the edges. (Ibrahimbegovic, Taylor, & Wilson, 1990)

3.2.3.1 Mesh size and loading

Three different full-shell models were created to be analyzed with thin-incompatible and thin-drilling shell elements (Figure 3-7 to Figure 3-9). Table 3-3 shows the dimensions of shell elements employed for the web and flanges. For the web, dimensions are given along the longitudinal and elevation axis of the member. For flanges, dimensions are given along the longitudinal and transverse axis of the member. The torsional load of 100 kip-in was modeled by a force couple applied to the flange nodes at the tip.

Table 3-3 Mesh sizes used in full-shell models.

	Web (in)		Flanges (in)	
	Along Length	Along Depth	Along Length	Along Width
Shell Model 1	20	17.32	20	8.235
Shell Model 2	10	8.66	10	8.235
Shell Model 3	5	4.33	5	4.1175

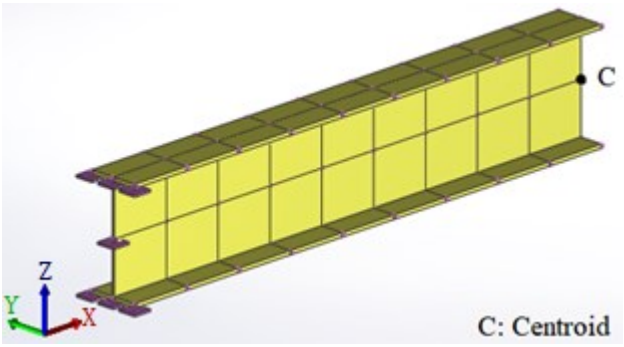

Figure 3-7 Shell Model 1: 54 elements.

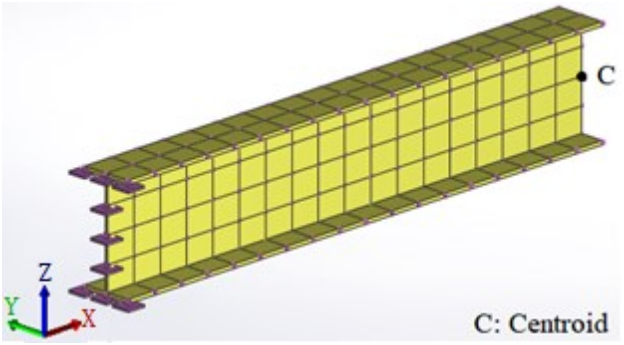

Figure 3-8 Shell Model 2: 144 elements.

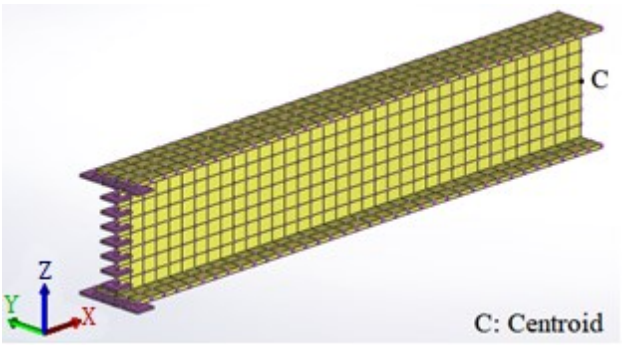

Figure 3-9 Shell Model 3: 576 elements.

3.2.3.2 Twist angles of full-shell models

The rotation-X values at the end of the member were extracted from the nodes of shell models defined at the centroid of the cross-section and compared with the analytical solution that was found to be 0.01609 radians, as shown in Table 3-4.

Table 3-4 Twist angle at the centroid (θ_x at x = L), in radians.

	Shell Model 1	Shell Model 2	Shell Model 3
Thin - Incompatible	0.01879 (15.5%)	0.01887 (15.9%)	0.01889 (16.0%)
Thin - Drilling	0.01873 (15.2%)	0.01881 (15.6%)	0.01888 (16.0%)

Note: The values in brackets are percentage differences between the analytical solution and shell model.

Since the Vlasov's theory assumes the cross-section to be undeformable in its own plane and neglects shear deformation effects, the twist angle values extracted from the shell models are larger than the twist angle value obtained from the analytical solution. While the Vlasov's theory assumes that the web remains straight during twisting, the previous research has shown that the web distorts during twisting as predicted by the refined finite-element analysis (Pezeshky, 2017).

In order to investigate the effect of these assumptions on the results, two more sets of analysis results were obtained by adding rigid link elements and flexurally rigid elements to the member end along the web depth. The rigid link elements introduce a rigid connection between the element's nodes in all directions, i.e., it does not deform but allows the relative rigid body movement of the nodes it connects. Hence, these elements restrain the shear deformations resulting from the bending (or warping) of flanges and the web distortion. This way, the member is enforced to behave in a similar manner as the assumption of Vlasov's theory. The flexurally rigid elements are conventional Timoshenko beam elements with a very large shear area and moment of inertia quantities. Therefore, these elements only restrain web distortion.

The updated results were reported in Table 3-5 and Table 3-6 for models with rigid links and flexurally rigid elements, respectively. Although the results of thin-incompatible shell models reported in both tables are in good agreement with the analytical solution, the thin-drilling shell models show stiffer behavior when used in combination with the rigid links. The main reason for this lies in the formulation of drilling DOF. In this element, the drilling rotation at a node is calculated from the

mid-edge displacements of the neighbor edges. When rigid links restrain the drilling rotations of nodes at the flange-web intersections, they also restrain the translation of the mid-edge displacements of the elements connecting to the node. This causes an additional stiffening effect for the bending of flanges caused by warping. That's why as the size of elements is reduced, this stiffening effect diminishes, and the results approach the analytical result.

Table 3-5 Twist angle at the centroid (θ_x at x = L) for restrained web distortion and shear deformation, in radians.

	Shell Model 1	Shell Model 2	Shell Model 3
Thin - Incompatible	0.01613 (0.2%)	0.01631 (1.4%)	0.01641 (2.0%)
Thin - Drilling	0.01301 (21.2%)	0.01470 (9.0%)	0.01549 (3.8%)

Note: The values in brackets are percentage differences between the analytical solution and shell model.

Table 3-6 Twist angle at the centroid (θ_x at x = L) for restrained web distortion, in radians.

	Shell Model 1	Shell Model 2	Shell Model 3
Thin - Incompatible	0.01637 (1.7%)	0.01655 (2.8%)	0.01665 (3.4%)
Thin - Drilling	0.01635 (1.6%)	0.01649 (2.5%)	0.01663 (3.3%)

Note: The values in brackets are percentage differences between the analytical solution and shell model.

Considering Table 3-5 and Table 3-6, it can be concluded that the differences between the analytical solution and results reported in Table 3-4 are mainly due to the web distortion. Figure 3-10, which is a plot of lateral web displacements at the end of the member with and without the rigid links, was obtained from the displacements of Shell Model 3 with thin-incompatible shell element type. This figure shows that the web does not remain straight during twisting, as opposed to the assumption of Vlasov's theory.

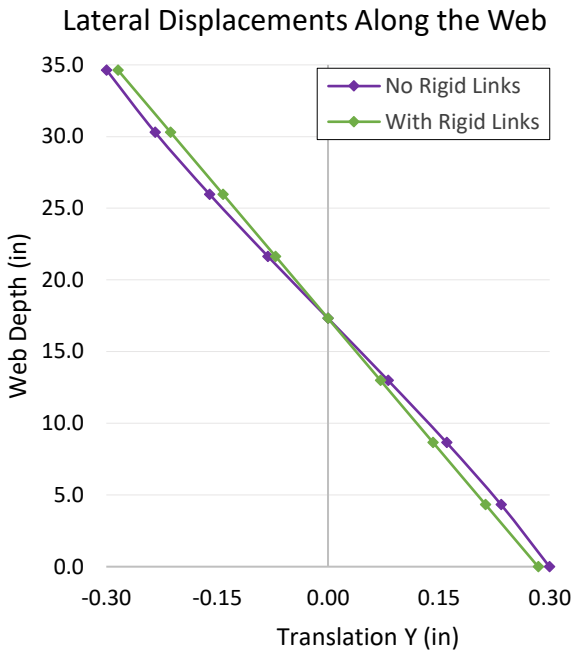

Figure 3-10 Shell Model 3: Lateral displacements along the web.

As a result, when no rigid links or flexurally rigid elements exist in the model, both thin-incompatible and thin-drilling shell elements produce similar results that are close to the actual behavior under torsional loading.

3.2.3.3 Refined model with shell elements

The element size of the Shell Model 2 and thin-incompatible shell type has been found adequate in producing accurate results and will be taken as a reference in the second verification problem, also in the case studies. The results along the length of the member were extracted from Shell Model 2 for thin-incompatible shell type with and without rigid links and compared with the analytical results. The rotation-X values of centroid nodes were extracted from the model, and variation of twist angle along the length of the member is presented in Figure 3-11. In order to obtain the variation of St.Venant Torsion presented in Figure 3-12, the rotation-Z values of flange middle nodes, i.e., in-plane flange mid-line rotations, were extracted from the

model and substituted into Equation 3-5, which can be derived by integrating Equation 2-4 and inserting into Equation 2-1.

$$M_s = GJ\frac{\theta_z}{\left(\frac{h}{2}\right)} \tag{3-5}$$

where G is the shear modulus, J is the torsion constant, θ_z is the in-plane flange mid-line rotation, and h is the distance between flange centroids.

In order to obtain the variation of warping torsion presented in Figure 3-13, the total torsion at the centroid of the cross-section was extracted from the model, and the St.Venant torsion was subtracted from the total torsion. The Compound Element Forces Tool of LARSA 4D program, which reports the combined forces and moments of a group of elements about their combined centroid, was utilized to extract the total torsion from the model.

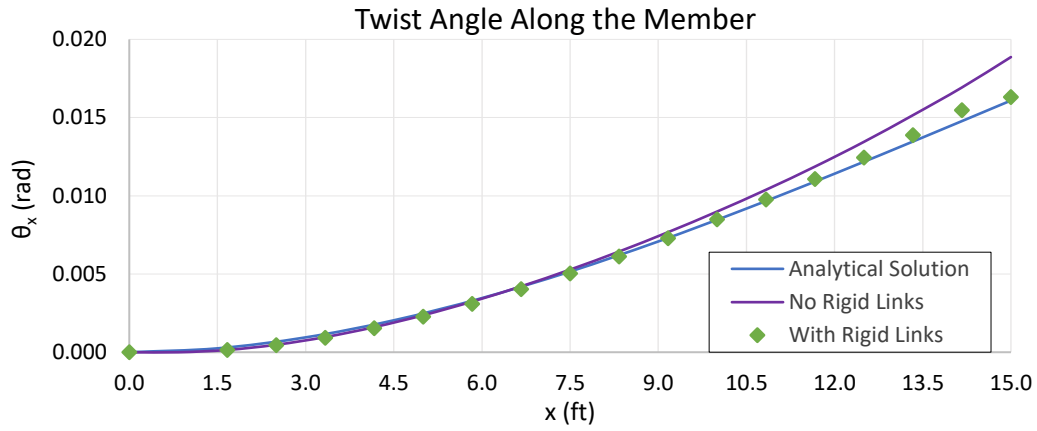

Figure 3-11 Refined Model: Twist angle along the member.

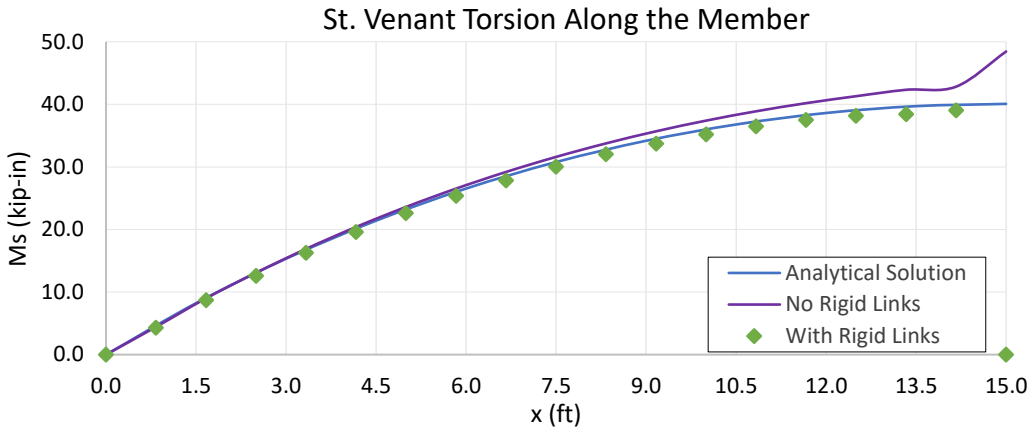

Figure 3-12 Refined Model: St. Venant torsion along the member.

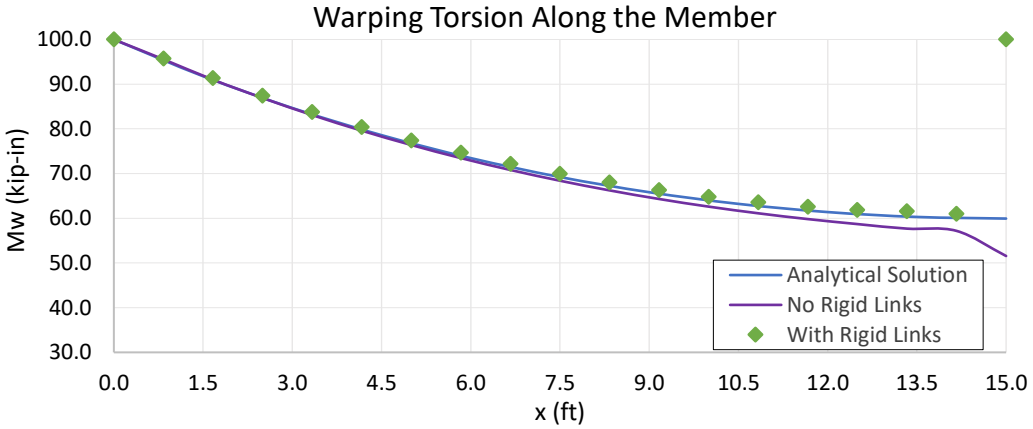

Figure 3-13 Refined Model: Warping torsion along the member.

In the presence of rigid links, the member behaves as assumed in Vlasov's theory, and the variation of results along the member length is in-line with the analytical solution. In Figure 3-12, the last value is zero at the member end because the rigid link elements at this location restrained the in-plane flange mid-line rotation that was used to compute the St.Venant torsion. Consequently, in Figure 3-13, the warping torsion at the end of the member is equal to the total torsion at the end of the member. Moreover, without rigid links, the jump seen in the force graphs at the end of the member is due to the applied force and reduces by smaller mesh size; therefore, it is neglected.

3.2.3.4 Alternative modeling: web with shell, flanges with beam elements

In the finite element analysis of steel I-section members, modeling the web of the cross-section with shell elements and flanges with beam elements is an alternative and practical modeling approach compared to full-shell models (Figure 3-14). In order to apply this approach, the flanges of I-beam were modeled with beam elements instead of a mesh of shell elements. The variation of twist angle and internal torsional moments along the member are reported from Figure 3-15 to Figure 3-17 for the alternative modeling approach, together with the results of the refined model. As can be seen from the figures, the alternative modeling approach is also capable of capturing the torsional response of the example structure and gives very similar results to the refined full-shell model.

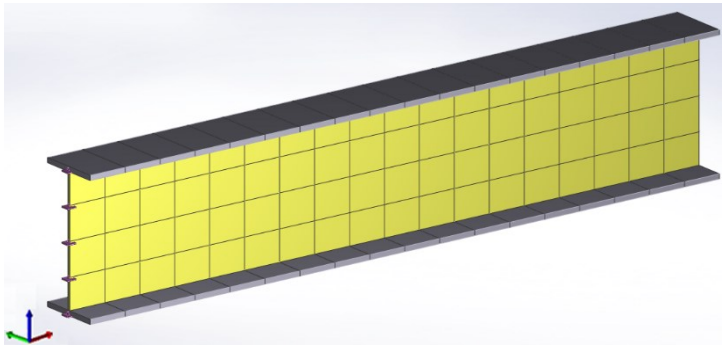

Figure 3-14 Shell Model 2: Alternative modeling.

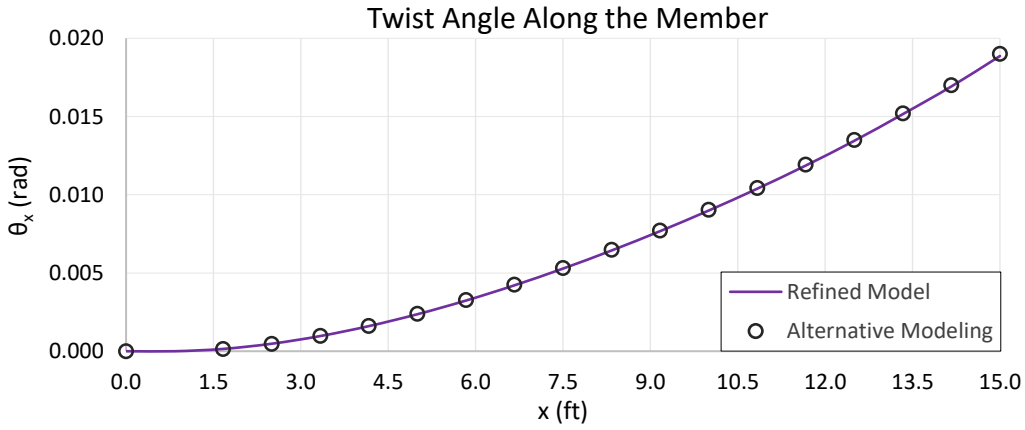

Figure 3-15 Alternative Modeling: Twist angle along the member.

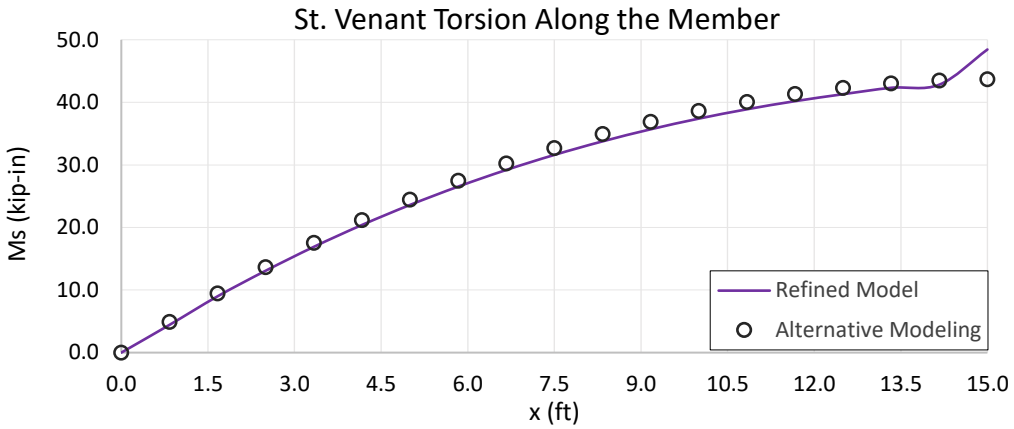

Figure 3-16 Alternative Modeling: St.Venant torsion along the member.

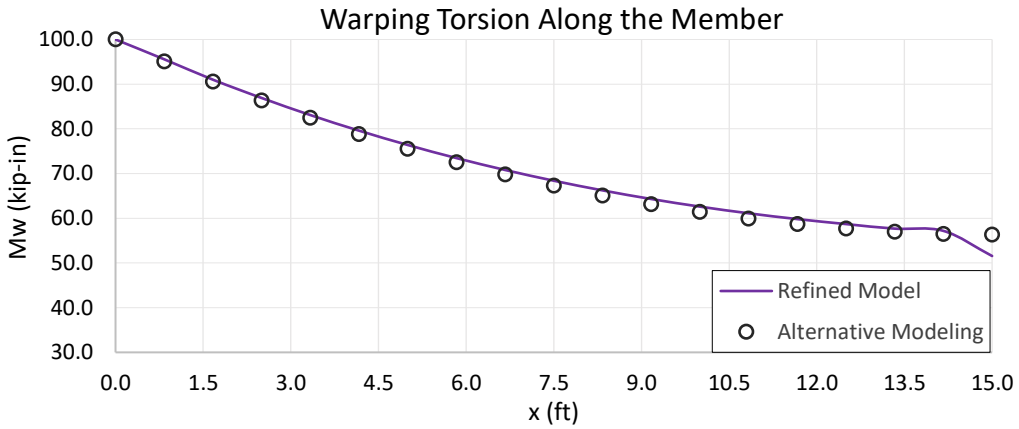

Figure 3-17 Alternative Modeling: Warping torsion along the member.

3.3 Verification Problem 2: Torsionally Fixed-Fixed Beam

The 15 ft long member having torsionally fixed boundary conditions at the ends, was subjected to $T = 1000$ kip-in concentrated torsional moment at the mid-span (Figure 3-18). The results of beam and shell models were compared with the analytical solution.

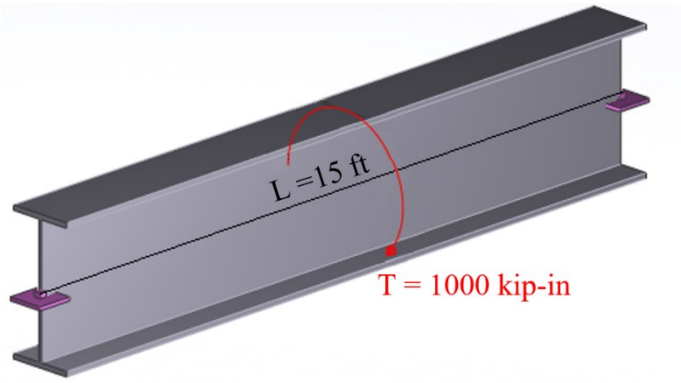

Figure 3-18 Geometry of Verification Problem 2.

3.3.1 Analytical solution

The boundary conditions of Verification Problem 2 dictate that the beam is not able to twist or warp at both ends:

$$\theta_x(x) = 0 \text{ at } x = 0 \text{ and } x = L \tag{3-6}$$

$$\theta'_x(x) = 0 \text{ at } x = 0 \text{ and } x = L \tag{3-7}$$

The solution of the general equation of torsional rotation, Equation 2-9, for this particular case is given by Equations 3-8 and 3-9 (Seaburg & Carter, 2003).

For $0 \leq x \leq L/2$

$$\theta_x = \frac{T}{(H+1) * GJk}\left\{\left[H * \left(\frac{1}{\sinh kL} + \sinh\frac{kL}{2} - \frac{\cosh\frac{kL}{2}}{\tanh kL}\right)\right.\right.$$
$$\left.\left. + \left(\sinh\frac{kL}{2} - \frac{\cosh\frac{kL}{2}}{\tanh kL} + \frac{1}{\tanh kL}\right)\right][\cosh kx - 1] - \sinh kx + kx\right\} \tag{3-8}$$

For $L/2 \leq x \leq L$

$$\theta_x = \frac{T}{\left(1 + \frac{1}{H}\right) * GJk}\left\{\left[\frac{\left(\cosh\frac{kL}{2} - 1\right)}{H * \sinh kL} + \frac{\left(\cosh\frac{kL}{2} - \cosh kL + kL * \sinh kL\right)}{\sinh kL}\right]\right.$$

$$+ \cosh kx * \left[\frac{\left(1 - \cosh\frac{kL}{2}\right)}{H * \tanh kL} + \frac{\left(1 - \cosh\frac{kL}{2} * \cosh kL\right)}{\sinh kL}\right]$$

$$\left. + \sinh kx * \left[\frac{\left(\cosh\frac{kL}{2} - 1\right)}{H} + \cosh\frac{kL}{2}\right] - kx\right\} \quad (3\text{-}9)$$

where $k = \sqrt{GJ/EC_w}$ and

$$H = \frac{\left[\frac{\left(1 - \cosh\frac{kL}{2}\right)}{\tanh kL} + \frac{\left(\cosh\frac{kL}{2} - 1\right)}{\sinh kL} + \sinh\frac{kL}{2} - \frac{kL}{2}\right]}{\left[\frac{\left(\cosh kL + \cosh\frac{kL}{2} * \cosh kL - \cosh\frac{kL}{2} - 1\right)}{\sinh kL} - \frac{kL}{2} - \sinh\frac{kL}{2}\right]} \quad (3\text{-}10)$$

The parameters M_s, M_w, and B are obtained by taking derivatives of θ_x and inserting into expressions given by Equations 2-1, 2-8, 2-5, respectively.

3.3.2 Beam models

The verification problem was solved in 3D Frame Analysis Program by utilizing 6 DOF beam elements with J_{eff} and 7 DOF warping beam elements. In order to analyze the mid-span loading, the verification problem was modeled utilizing two beam elements with J_{eff}. Since the warping boundary conditions are known only at the ends of the structure, the effective torsion constant was computed for the full member length of 15 ft, assuming the fixed-fixed boundary condition and used for both beam elements. The twist angle is the output parameter included in the reported results.

The results of the analytical solution and 3D Frame Analysis Program are presented in Table 3-7.

Table 3-7 Analysis results at L/2 and L/5.

	Analytical Solution	2 Beam Elements with J_{eff}	2 Warping Beam Elements	10 Warping Beam Elements
θ_x (rad) at x = L/2	0.00362	0.01329	0.00362	0.00362
M_s (kip-in) at x = L/5	17.60	-	-	17.60
M_w (kip-in) at x = L/5	482.40	-	-	482.40
B (kip-in^2) at x = L/2	21949	-	21949	21949

According to the results shown in Table 3-6, the warping beam formulation gives exactly the same results with the analytical solution. The use of the same J_{eff} for the elements between known warping boundary conditions is an approximation, and it did not produce an acceptable solution.

From Figure 3-19 to Figure 3-22, the variation of displacements and forces along the member were plotted on the same graph for the analytical solution and warping beam elements. As can be seen from the figures, the analysis results extracted from the intermediate elements are also in line with the analytical solution. At the fixed ends and loaded mid-span, the total torsion is entirely carried by the warping torsion, and the bi-moment is at its maximum. Both warping torsion and bi-moment decrease towards the quarter span from both ends. However, even at the point where the St. Venant torsion is maximum, i.e., at 3.75 ft, the ratio of St.Venant torsion to warping torsion is only 3.6%.

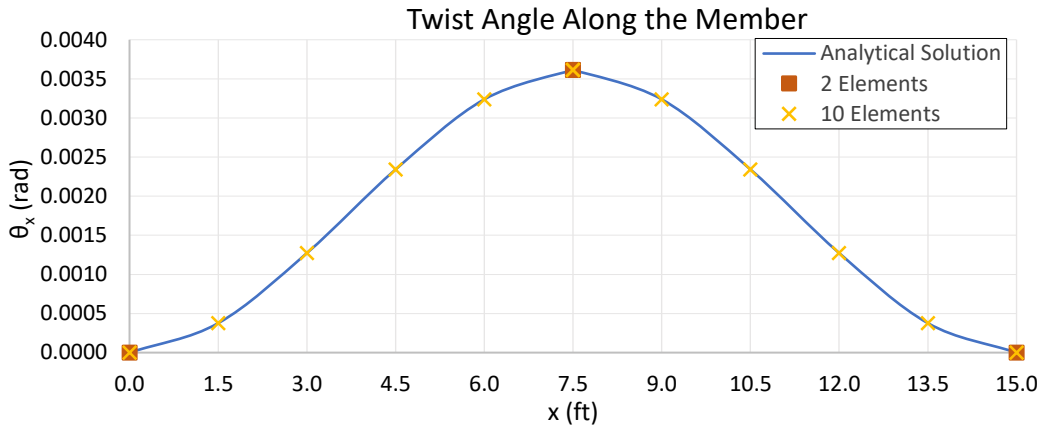

Figure 3-19 Verification Problem 2: Twist angle along the member.

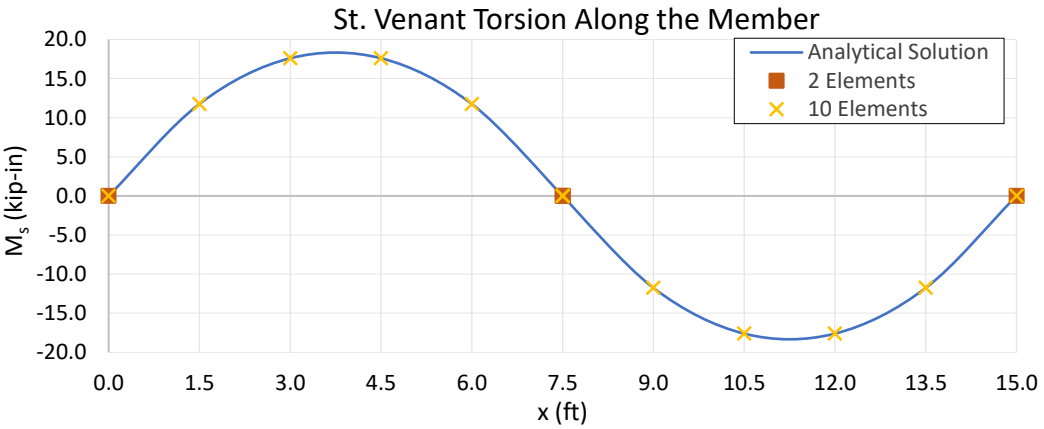

Figure 3-20 Verification Problem 2: St. Venant torsion along the member.

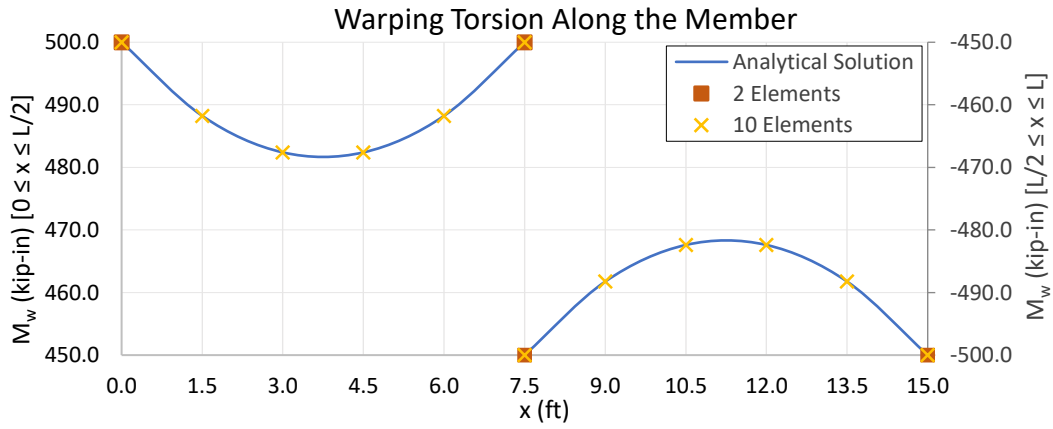

Figure 3-21 Verification Problem 2: Warping torsion along the member.

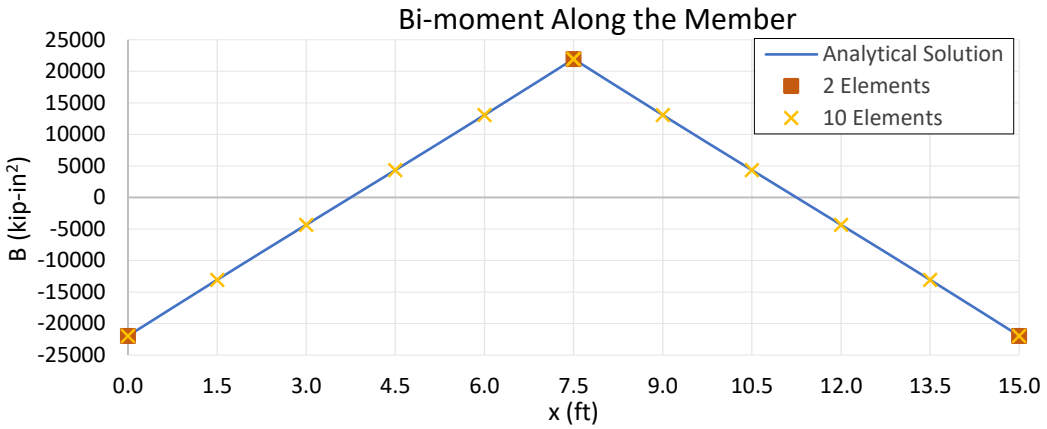

Figure 3-22 Verification Problem 2: Bi-moment along the member.

3.3.3 Shell models

The same problem was modeled with shell elements by using the same mesh size and element type as the refined model of Verification Problem 1 (Shell Model 2, Figure 3-8). The fully-fixed boundary conditions were assigned to the nodes at both ends, and the torsional load of 1000 kip-in was modeled by a force couple applied to the flange nodes at the mid-span.

Since Vlasov's theory neglects web distortion and shear deformation effects, the twist angle values of the refined full-shell model are expected to be larger than the analytical solution. Similar to the Verification Problem 1, additional models were created to investigate the effect of these assumptions by adding rigid link elements restraining the shear deformations and web distortion, and flexurally rigid elements restraining only the web distortion, to the model. Different from Verification Problem 1, where the rigid elements were defined only at the beam end, these elements were defined in Verification Problem 2 throughout the beam. The twist angle values at the mid-span were extracted from the nodes of shell models defined at the centroid of the cross-section and compared with the analytical solution, that was found to be 0.0036 radians, as shown in Table 3-8.

Table 3-8 Twist angle at the mid-span (θ_x at x = L/2), in radians.

No Rigid Element	With Flexurally Rigid Elements	With Rigid Link Elements
0.0043 (17.7%)	0.0039 (8.0%)	0.0037 (2.7%)

Note: The values in brackets are percentage differences between the analytical solution and shell model.

The percentage differences between the analytical solution and shell models show the same trend as the previous verification problem (Table 3-4 to Table 3-6). For both verification problems, when there are no rigid elements in the model, the percentage difference between the analytical solution and the shell model is around 16-17%. While the contribution of shear deformation effects to the percentage difference is more pronounced in the current verification problem, the differences between the analytical solution and extracted results are found to be mainly due to the web distortion, similar to the previous verification problem.

The variation of twist angle values extracted from the centroid nodes along the member is presented in Figure 3-23. The variation of St.Venant torsion and warping torsion, which are obtained based on the in-plane flange mid-line rotations, are presented in Figure 3-24 and Figure 3-25. In Figure 3-23, the twist angle values extracted from the full-shell model with rigid link elements are included. Results of the alternative modeling approach, in which flanges of the cross-section are modeled with beam elements, are also presented in these graphs.

In the presence of rigid links, the member behaves as assumed in Vlasov's theory, and the variation of twist angle along the member length is in-line with the analytical solution. Unlike the twist angle, it was observed that the variation of St. Venant torsion and warping torsion are not affected by the assumptions of Vlasov's theory. In addition, the alternative modeling approach is found to be capable of capturing the torsional response of the example structure as it produces the results similar to the refined full-shell model.

Figure 3-23 Shell Models: Twist angle along the member.

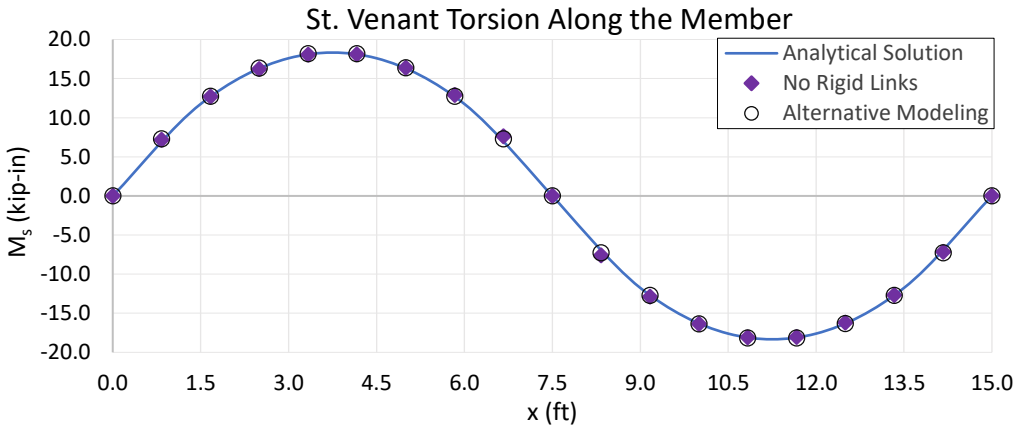

Figure 3-24 Shell Models: St. Venant torsion along the member.

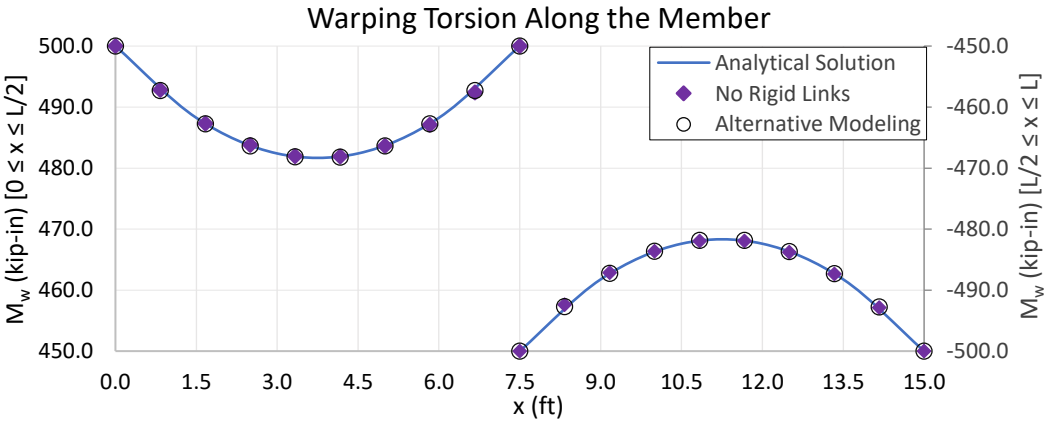

Figure 3-25 Shell Models: Warping torsion along the member.

CHAPTER 4

CASE STUDIES

During the construction of steel I-girder bridges, exterior girders are subjected to torsional moments that are produced by the eccentric loads acting on the overhang forming brackets. The loads include the weight of deck overhang concrete, deck form, screed rail, and finishing machine. In the analysis and design of exterior girders, it is necessary to consider the flange lateral bending moments and stresses resulting from these torsional loads. In addition to the eccentric overhang bracket loads, the girders of horizontally-curved steel I-girder bridges are subjected to torsion under vertical construction loads. The flange lateral bending moments and stresses due to curvature should also be considered in the analysis and design of these bridges.

As an example of the design code requirement, the effects of eccentric overhang bracket loads acting on the non-composite exterior I-girders should be investigated at the Constructibility Limit State per AASHTO LRFD Bridge Design Specifications, Article 6.10.3.4 – Deck Placement (American Association of State Highway and Transportation Officials, 2017). In the commentary section of this article, two equations are suggested to estimate the maximum flange lateral bending moments, M_{lat}, under the loadings mentioned in the preceding paragraph, and the equations are to be used in the absence of a more refined analysis. Both equations are based on the assumption that adjacent unbraced lengths have approximate symmetry conditions, and hence torsionally fixed boundary conditions exist at the ends of the unbraced length. Equation 4-1 is suggested for the case of the eccentric overhang loading assumed to be applied as uniformly distributed lateral loads, F_{lat}, to the flanges.

$$M_{lat} = \frac{F_{lat} * {L_b}^2}{12} \quad (4\text{-}1)$$

where L_b is the unbraced length.

Per AASHTO LRFD Bridge Design Specifications, Article 6.10.3.2 – Flexure, the flange lateral bending effects due to curvature must always be considered in discretely braced flanges during construction. In the commentary section of Article 4.6.1.2.4b – I-Girders, the specification provides an approximate equation (Equation 4-2) to be used for determining the lateral bending moment due to curvature. The equation is based on the V-Load Method (Fiecht, Fenves, & Frank, 1987), which assumes the presence of a cross-frame at the point under consideration to resist the torsional action due to curvature by sets of shears developed within the cross-frames. The method also assumes the uniform cross-frame spacing and constant major-axis bending moment, M, within the unbraced length, L_b.

$$M_{lat} = \frac{M * {L_b}^2}{N * R * D} \quad (4\text{-}2)$$

where R is the girder radius, D is the web depth, and N is a constant taken as 10 or 12.

In addition to the stresses resulting from the major-axis bending effects, the flange lateral bending stresses resulting from the curvature for curved girders as well as the flange lateral bending stresses resulting from the overhang bracket loads for exterior girders are considered when checking the flexural resistance of discretely braced flanges at the Constructibility Limit State, per AASHTO LRFD Bridge Design Specifications, Article 6.10.3.2 – Flexure.

Furthermore, excessive rotation of exterior girders under the overhang bracket loads may cause a considerable amount of deck thickness loss leading to overstress in the girders, and such problems may also be encountered during the deck placement. In order to limit the girder rotation, it is necessary to predict the twist angle of the exterior girder accurately. For example, the Illinois Department of Transportation

(IDOT) limits the maximum vertical displacement of the overhang tip to 3/16 inches, and the exterior girder rotation corresponding to that displacement can be treated as the limit (Ashiquzzaman et al., 2016).

Apart from these, the steel girders are cambered during the fabrication to compensate for the dead load deflections and match the designed profile in the final state. In case the finite element method is used for the analysis and estimating the camber information, it is essential to capture girder vertical deflections precisely. Since the horizontally-curved girders are under the coupled action of major-axis bending and torsion for the dead load effects, the torsional modeling has a significant effect on vertical deflection values.

In order to understand what extend the beam element formulations with warping, refined, and alternative modeling approaches can produce accurate analysis results and to qualify the usability of the proposed modeling approaches in the current bridge engineering practice, three case studies are conducted by focusing on the specified load effects and design parameters. As a first case study, a straight exterior I-girder is analyzed under deck overhang loads. As a second case study, a single horizontally-curved I-girder is analyzed under deck weight loading. As a third case study, a single span horizontally-curved I-girder bridge superstructure is analyzed under deck weight loading.

A comparative study is performed for all case studies. The 3D full-shell models and alternative shell models, in which flanges of the cross-section are modeled with beam elements, are constructed and analyzed in LARSA 4D program. Beam models are constructed and analyzed in 3D Frame Analysis Program by utilizing 6 DOF conventional beam elements, 6 DOF beam elements with an effective torsion constant (J_{eff}), and 7 DOF warping beam elements, for the girder. The results of different modeling approaches are compared by taking the 3D full-shell model as a reference. For all case studies, the existing bridge geometries were considered in the generation of analysis models.

4.1 Case Study #1: Straight Exterior I-Girder Under Overhang Loads

A 130 ft long simply supported straight I-girder was modeled as an isolated exterior girder by using flat shell and beam elements. The cross-sectional dimensions of the girder are shown in Figure 4-1. The sectional and material properties used in the analysis are given in Table 4-1.

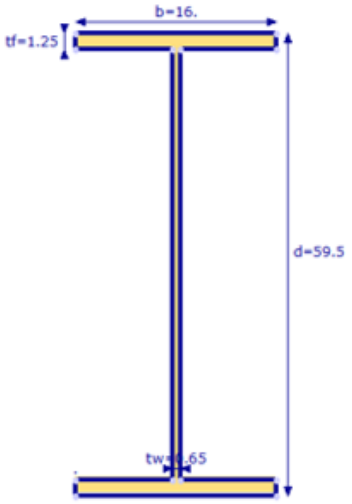

Depth (d) = 59.5 in

Width (b) = 16.0 in

Flange Thickness (tf) = 1.25 in

Web Thickness (tw) = 0.65 in

Figure 4-1 Straight Exterior Girder: Cross-sectional dimensions.

Table 4-1 Straight Exterior Girder: Properties.

Cross-Sectional Properties	
Area (A)	77.05 in^2
Moment of inertia about the z-axis (I_z)	43967.12 in^4
Moment of inertia about the y-axis (I_y)	854.6378 in^4
Torsion constant (J)	26.56 in^4
Warping constant (C_w)	723740 in^6
Material Properties	
Modulus of elasticity (E)	29000 ksi
Shear modulus (G)	11200 ksi

4.1.1 Deck overhang loads

The overhang width and the average deck thickness in the overhang were taken as 3.25 ft and 9 inches, respectively. The unit weight of concrete used in the self-weight computation is 150 lb/ft^3. The total deck overhang weight was calculated as 366 lb/ft. The half of deck overhang weight was assumed to be resisted by overhang brackets and the other half by the girder. The weight of deck forms and screed rail included in overhang bracket loads is 185 lb/ft. The analyzed loads are summarized in Figure 4-2. While the loads were analyzed as uniform member loads in beam models, they were analyzed as nodal loads in shell models.

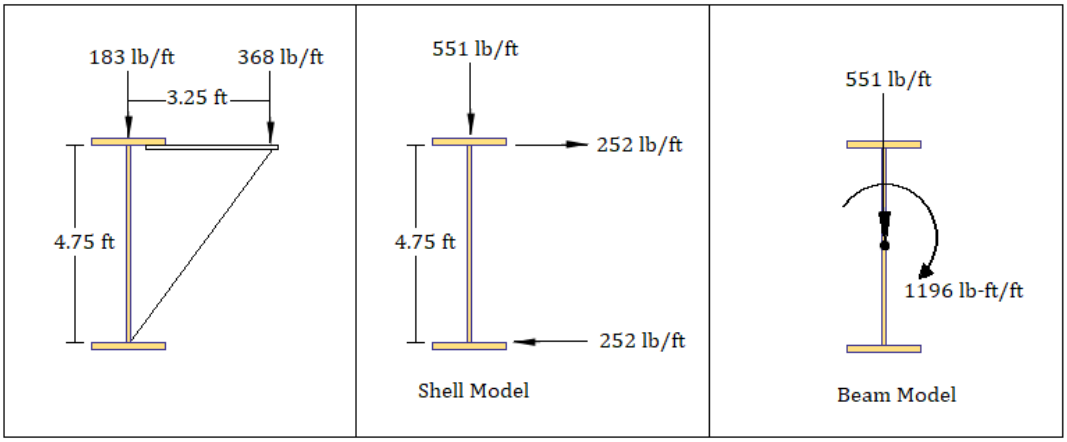

Figure 4-2 Deck overhang loads.

4.1.2 Analysis models

The sample exterior girder was modeled in LARSA 4D finite element analysis software with flat shell elements. In addition to full-shell models, flanges of I-girder were modeled with beam elements, and the results of this alternative modeling approach were included in the comparison. The same problem was solved in 3D Frame Analysis Program by utilizing the different beam elements available in the program. The laterally supporting cross-frames were not modeled explicitly. Instead, the torsional restraints were provided in beam models, and the lateral restraints were

provided in shell models. The assumed eight cross-frame locations, including the start and end of the girder, are shown in Figure 4-3.

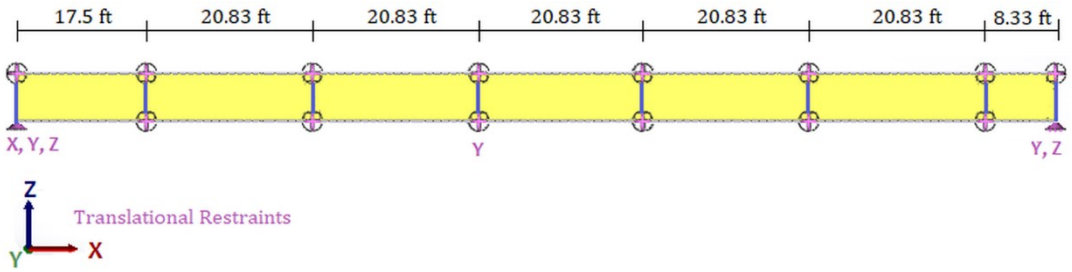

Figure 4-3 Side View: Cross-frame locations.

In shell models, the simple supports at girder ends were defined at the bottom flange nodes. As stated in Chapter 3, the thin-incompatible shell-type was utilized in all case studies. The dimensions of shell elements employed for the web is 10 inches × 9.7 inches along the longitudinal and elevation axis of the girder, respectively. The dimensions of shell elements employed for flanges are 10 inches × 8 inches along the longitudinal and transverse axis of the girder, respectively.

In beam models, each unbraced length was divided into four beam elements, except for the 8.33 ft long last segment, which was divided into two elements. The simple supports at girder ends were defined at the centroid.

All the analysis models of the first case study are summarized in Table 4-2.

Table 4-2 Analysis models of the first case study.

Analysis Models	
Shell Model 1 (SM1):	Full-shell (reference) model. Web distortion is prevented at cross-frame locations with rigid members.
Shell Model 2 (SM2):	The web is modeled as shell elements, flanges are modeled as beam elements. Web distortion is prevented at cross-frame locations with rigid members.
Shell Model 3 (SM3):	Full-shell model. Connection plates are modeled at cross-frame locations.
Shell Model 4 (SM4):	The web is modeled as shell elements, flanges are modeled as beam elements. Connection plates are modeled at cross-frame locations as beam elements.
Beam Model 1 (BM1):	Beam model with 7 DOF warping beam elements.
Beam Model 2 (BM2):	Beam model with 6 DOF beam elements and J_{eff}.
Beam Model 3 (BM3):	Beam model with conventional 6 DOF beam elements.

When setting up the BM2 model, assumptions were made regarding warping deformations. The warping was assumed to be free at the simply supported ends of the girder and restrained at cross-frame locations except for the last cross-frame location considering that the length of each span is same or close to each other except the last span. For the first six members, the effective torsion constant was computed using the member's unbraced length and boundary conditions as either free or fixed. Since there is a significant difference between the lengths of the last two members, the effective torsion constant (J_{eff}) was not computed in a similar manner. Instead, the torsion constant of the girder cross-section given in Table 4-1 was utilized in the analysis.

The full-shell model SM1 was taken as the reference model for comparisons. While generating SM1 and SM2 models, flexurally rigid members were added along the web depth at cross-frame locations assuming that the connection plates at these locations prevent the web distortion. The models SM3 and SM4 were created additionally to test the effect of the flexible connection plate. The 0.65 inches thickness full-depth connection plate was modeled on single-side of the exterior

girder except for the girder ends, which have double-sided plates to represent the bearing stiffeners, as shown in Figure 4-4.

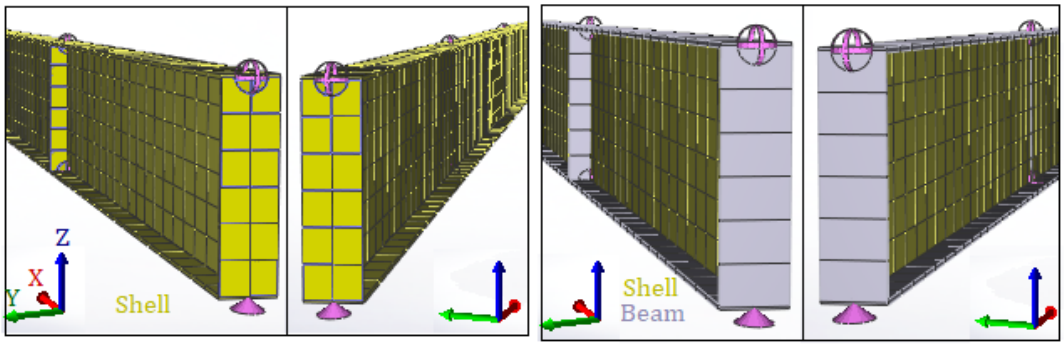

Figure 4-4 Analysis models SM3 and SM4 with connection plates.

4.1.3 Major-axis bending

For the major-axis bending response, all analysis models produced the same results. The mid-span deflection was obtained as 2.81 inches in the downward direction. At support locations, the magnitude of equal and opposite rotations was 0.0057 rad about the transverse axis of the girder.

4.1.4 Twist angle

In Figure 4-5, the twist angle values obtained from the shell models SM1, SM2, and warping beam model BM1 are plotted on the same graph. The shell model SM2, where the flanges of the girder were modeled with beam elements, produced the same results as the reference full-shell model, SM1. The twist angle values within the unbraced length of shell models are larger than the warping beam model, which shows that the web distortion is effective within the unbraced length of the girder. Since the web distortion was prevented at cross-frame locations, the zero twist angle computed at the beam ends in the warping beam model is also seen in the shell models.

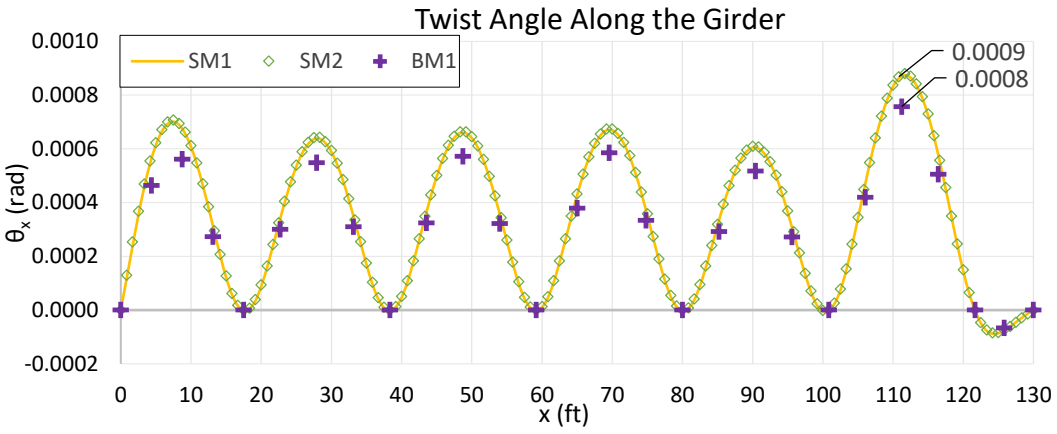

Figure 4-5 Twist angle along the girder for models SM1, SM2, and BM1.

The results obtained from beam models BM2 and BM3 are plotted separately in Figure 4-6, together with the results of the reference model SM1. While the use of J_{eff} in the analysis of beam model BM2 improves the results, considering the twist angle values in the middle of each unbraced length, it can be seen that the results of the BM2 model are three to eight times larger than the reference model SM1. This is because the J_{eff} is computed based on the assumptions made regarding warping deformations at the ends of each unbraced length, and the same J_{eff} value is employed for intermediate elements since the warping boundary conditions within the unbraced length are unknown. For the BM3 model, the twist angle goes up to thirty to fifty times the reference model as a result of neglecting the warping effects. Another factor contributing to these differences is that the beam elements of BM2 and BM3 models are not capable of capturing the web distortion effects, similar to the beam elements of the BM1 model.

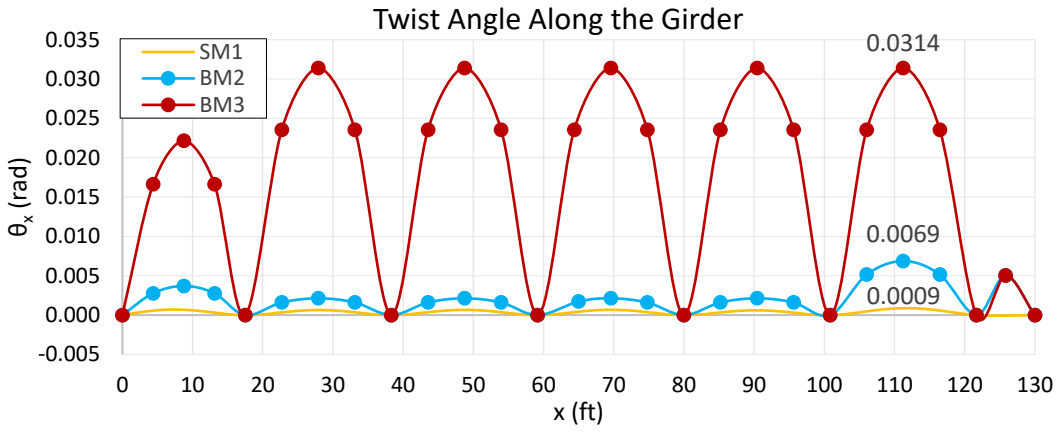

Figure 4-6 Twist angle along the girder for models SM1, BM2, and BM3.

In Figure 4-7, the results obtained from shell models SM3 and SM4 are plotted together with the results of reference model SM1. Modeling of the flexible connection plates did not make a significant difference in the results when compared to the reference model in which the web distortion is fully prevented at the cross-frame locations. The difference at the intermediate cross-frame locations is due to the eccentricity between single-sided connection plates and the vertical loads applied on top flange along the centroidal axes of the girder. The effect of additional torsion induced by this eccentricity is seen in the twist angle results. The largest difference is seen at the fourth cross-frame location, i.e., 59.16 ft, and it is equal to 0.0001 radians.

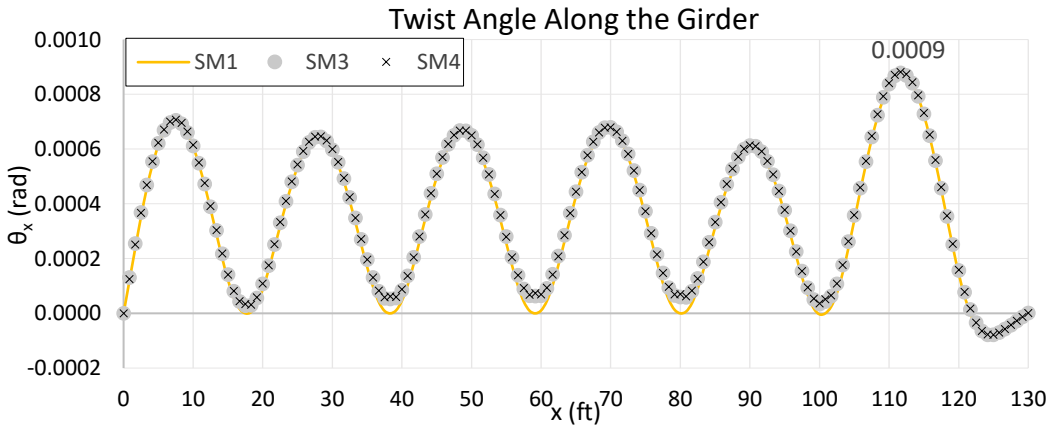

Figure 4-7 Twist angle along the girder for models SM1, SM3, and SM4.

For the 3.25 ft overhang width of the present case study, the 3/16 inches maximum vertical deflection limit for the overhang tip suggested by IDOT is equivalent to 0.0048 rad rotation limit for the girder. Considering Table 4-3, it is apparent that the twist angle values obtained from the models with conventional 6 DOF beam element and beam element with J_{eff} cannot be used to evaluate the beam rotation against the recommended limit, as it is overestimated. Whereas, the analysis model with warping beam elements produced reliable results.

Table 4-3 Maximum rotation θ_x obtained from analysis models.

Analysis Model	Maximum Rotation θ_x (rad)
SM1-SM4	0.0009
BM1	0.0008
BM2	0.0069
BM3	0.0314

4.1.5 Lateral bending

The lateral bending moments were extracted from the individual flanges of girder shell models and reported separately for the top and bottom flanges. While the 6 DOF beam elements do not give any output regarding the flanges, the 7 DOF warping beam element produces bi-moments as a component of member forces. The equal and opposite flange lateral bending moments for the torsional action were obtained by dividing the bi-moment output of the warping beam element by the distance between flange centroids. The results were plotted in Figure 4-8 and Figure 4-9, together with the results of shell models SM1 and SM2. As can be seen from these figures, the warping beam model BM1 and the shell model SM2, which uses an alternative modeling approach for the flanges, are able to capture the response of the reference model, SM1.

Additionally, it is observed that modeling of flexible connection plates has a negligible effect on the flange lateral bending moments, as can be seen in Figure 4-10 and Figure 4-11.

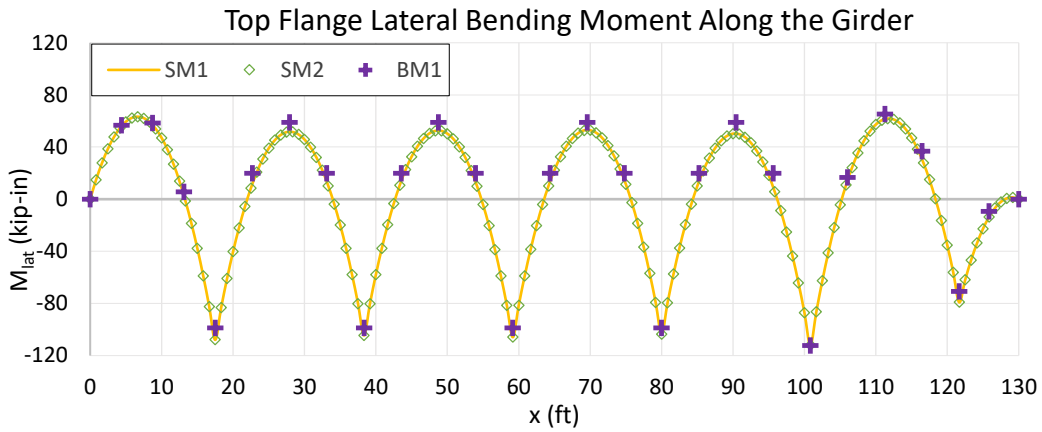

Figure 4-8 Top flange lateral bending moment. Models SM1, SM2, and BM1.

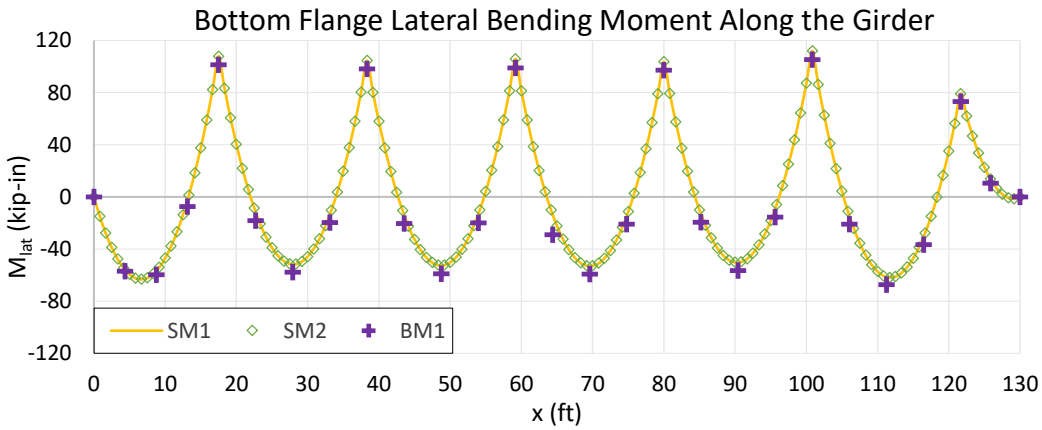

Figure 4-9 Bottom flange lateral bending moment. Models SM1, SM2, and BM1.

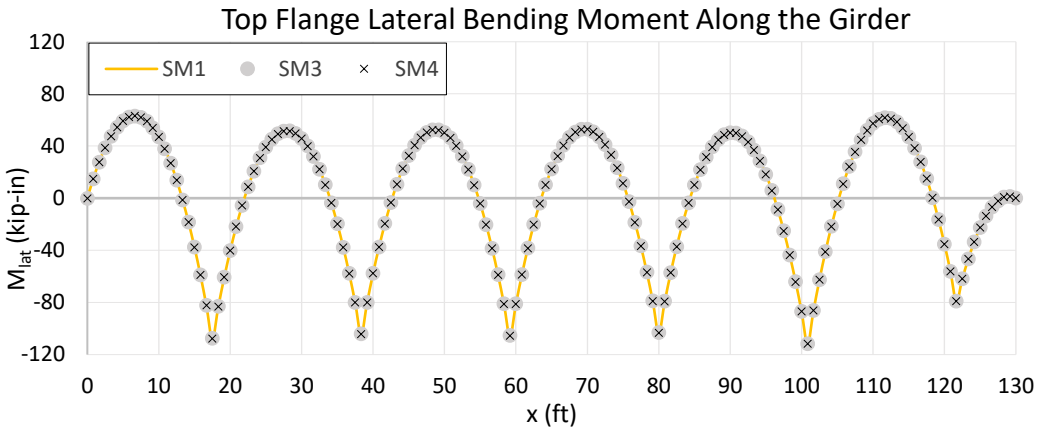

Figure 4-10 Top flange lateral bending moment. Models SM1, SM3, and SM4.

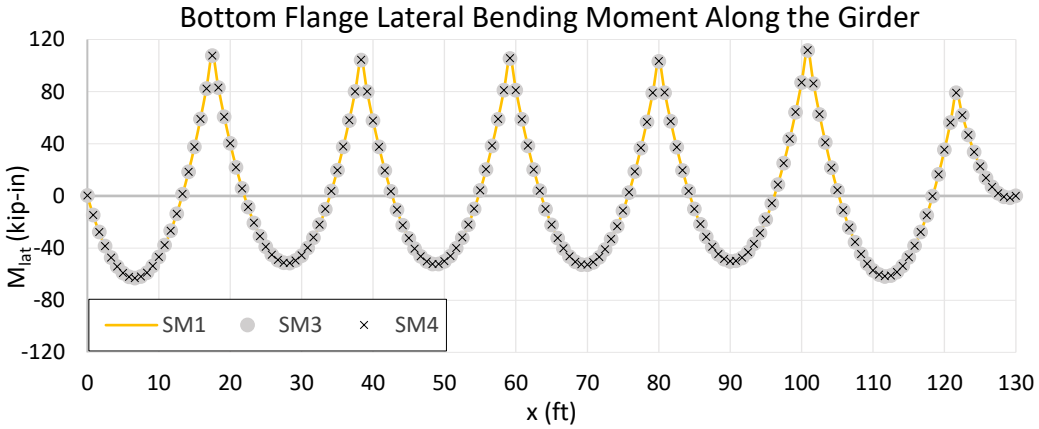

Figure 4-11 Bottom flange lateral bending moment. Models SM1, SM3, and SM4.

In Table 4-4, maximum absolute flange lateral bending moment values corresponding to 17.5 ft-long first segment, 20.83 ft-long intermediate segments, and 8.33 ft-long last segment are summarized together with the maximum moment values calculated by the approximate equation (Equation 4-1) suggested by AASHTO LRFD Bridge Design Specifications. When compared to the reference model SM1, all other analysis models produced close results. Since the approximate equation assumes torsionally fixed boundary conditions at the ends of unbraced length, it should not be used for the end segments.

Table 4-4 Maximum flange lateral bending moment within the unbraced length, in kip-in.

L_b	AASHTO LRFD C6.10.3.4.1-2	SM1	SM2	SM3	SM4	BM1
17.50 ft	77.2	107.9	107.8	107.6	107.6	101.3
20.83 ft	109.4	112.0	111.9	111.6	111.7	105.2
8.33 ft	17.5	79.2	79.1	79.1	79.0	73.0

4.1.6 Cross-frame forces

The laterally supporting cross-frames were represented by torsional restraints in beam models and by lateral restraints in shell models. To compare the lateral forces at the top and bottom chord of the cross-frames, the lateral support reactions were directly taken from the shell models, and the torsional support reactions obtained from the beam models were divided by the distance between flange centroids. The comparison of the results can be seen in Figure 4-12 and Figure 4-13.

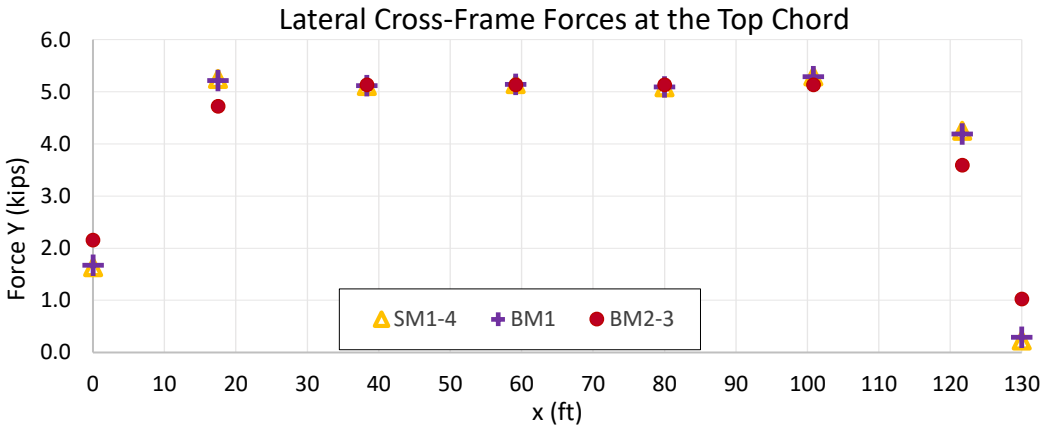

Figure 4-12 Lateral cross-frame forces at the top chord.

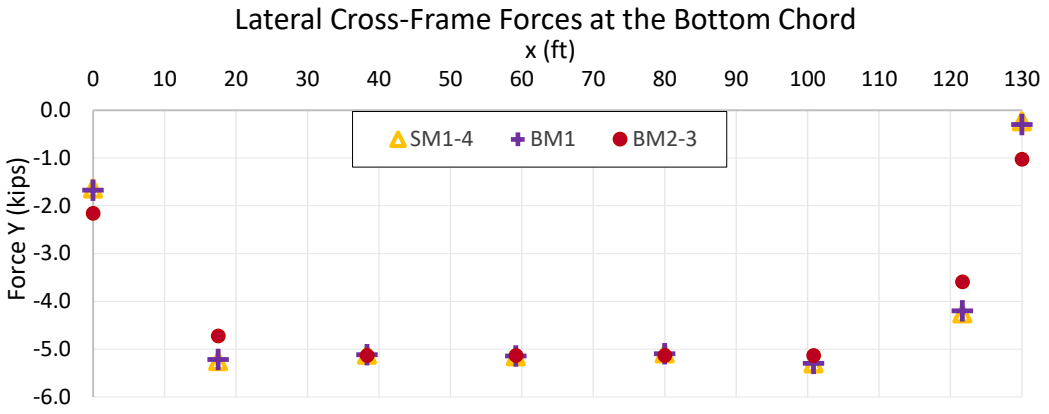

Figure 4-13 Lateral cross-frame forces at the bottom chord.

While reporting results, the results of all shell models and the results of beam models with 6 DOF were grouped together because they gave the same results. In all shell models, equal and opposite lateral forces developed in the top and bottom chord against the torsional action. The warping beam model, BM1, was able to capture the distribution of forces as shell models. The absence of a warping degree of freedom in the 6 DOF beam elements caused the torsional restraints in beam models BM2 and BM3 to develop reaction forces as in the case of warping-fixed boundary conditions defined together with torsional restraints.

4.2 Case Study #2: Horizontally Curved I-Girder Under Deck Weight Loading

A 150.5 ft long simply supported horizontally curved I-girder with 425 ft radius was modeled as an isolated interior girder by using flat shell and beam elements. The cross-sectional dimensions of the girder are shown in Figure 4-14. The sectional and material properties used in the analysis are given in Table 4-5.

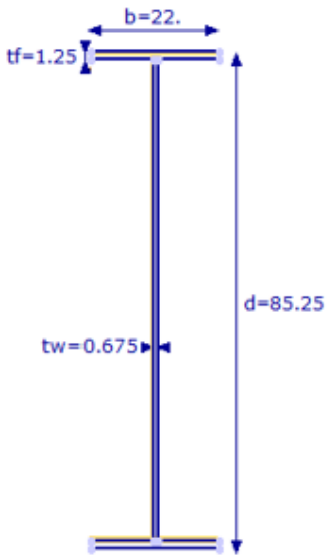

Depth (d) = 85.25 in

Width (b) = 22.0 in

Flange Thickness (tf) = 1.25 in

Web thickness (tw) = 0.675 in

Figure 4-14 Curved Interior Girder: Cross-sectional dimensions.

Table 4-5 Curved Interior Girder: Properties.

Cross-Sectional Properties	
Area (A)	110.86 in^2
Moment of inertia about the z-axis (I_z)	128900.43 in^4
Moment of inertia about the y-axis (I_y)	2220.45 in^4
Torsion constant (J)	38.97 in^4
Warping constant (C_w)	3912900 in^6
Material Properties	
Modulus of elasticity (E)	29000 ksi
Shear modulus (G)	11200 ksi

4.2.1 Deck weight loading

The deck thickness, including integral wearing surface and the tributary deck width, were taken as 9.5 inches and 8 ft, respectively. The unit weight of concrete used in the self-weight computation is 150 lb/ft^3. The deck weight was calculated as 950 lb/ft and applied as uniform member loads in beam models. In shell models, the loading was applied as nodal loads on top of girders.

4.2.2 Analysis models

The sample interior girder was modeled and analyzed in LARSA 4D finite element analysis software, also in 3D Frame Analysis Program, following similar procedures as the previous case study. The laterally supporting cross-frames were not modeled explicitly. Instead, the torsional restraints along the girder longitudinal axis were defined in beam models, and the lateral restraints along the girder transverse axis were provided in shell models. As shown in Figure 4-15, cross frames were assumed equally spaced at 21.5 ft along the girder, including the start and end of the girder. The girder was restrained in all translational directions at the start, in girder transverse and elevation axes at the end.

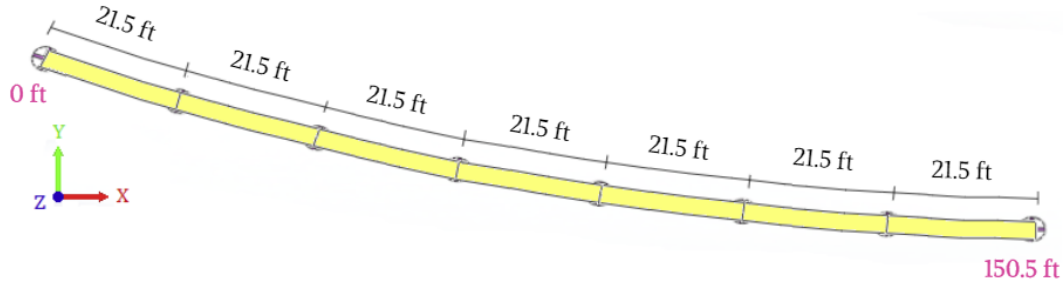

Figure 4-15 Plan View: Cross-frame locations.

In shell models, the pin supports at girder ends were defined at the bottom flange nodes. The dimensions of the shell elements employed for the web is 10.75 inches and 8.4 inches along the longitudinal and elevation axis of the girder, respectively. The dimensions of shell elements used for the flanges are 10.75 inches and 11 inches along the longitudinal and transverse axis of the girder, respectively.

In beam models, each unbraced length was divided into ten beam elements. The simple supports at girder ends were defined at the centroid.

All the analysis models of the second case study are summarized in Table 4-6.

Table 4-6 Analysis models of the second case study.

Analysis Models	
Shell Model 1 (SM1):	Full-shell (reference) model. Web distortion is prevented at cross-frame locations using rigid members.
Shell Model 2 (SM2):	The web is modeled as shell elements, flanges are modeled as beam elements. Web distortion is prevented at cross-frame locations using rigid members.
Beam Model 1 (BM1):	Beam model with 7 DOF warping beam elements.
Beam Model 2 (BM2):	Beam model with 6 DOF beam elements and J_{eff}.
Beam Model 3 (BM3):	Beam model with conventional 6 DOF beam elements.

When setting up the BM2 model, the warping condition was assumed to be free at the simply supported ends of the girder and restrained at the cross-frame locations. The effective torsion constant was computed for each unbraced length and applied to all beam elements within the unbraced length.

The full-shell model SM1 (Figure 4-16) was taken as the reference model in comparisons. Similar to the previous case study, flexurally rigid members were added along the web depth at the cross-frame locations. Since the effect of modeling flexible connection plates was found to be negligible in the previous case study, there is no additional analysis model created to consider this effect in the present case study.

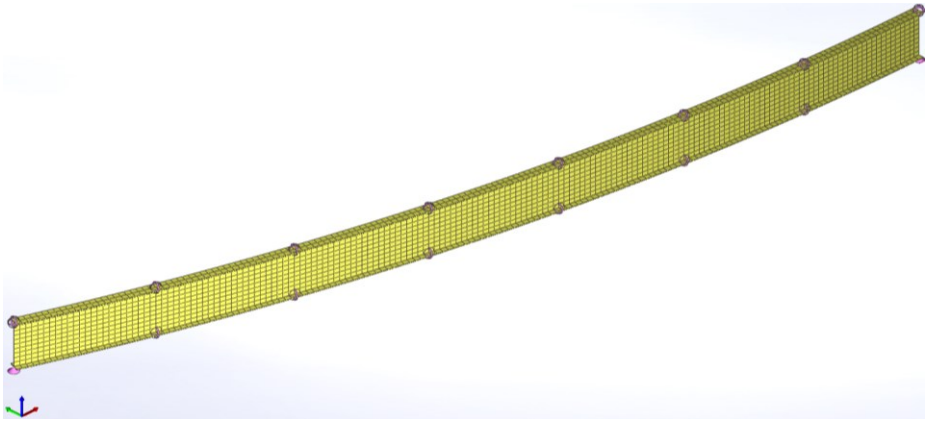

Figure 4-16 3D View: The full-shell model.

4.2.3 Major-axis bending

For the major-axis bending response, all analysis models produced almost the same results except the BM3 model with conventional 6 DOF beam elements. In Figure 4-17 and Figure 4-18, the vertical displacement and rotation about the girder transverse axis are plotted along the girder.

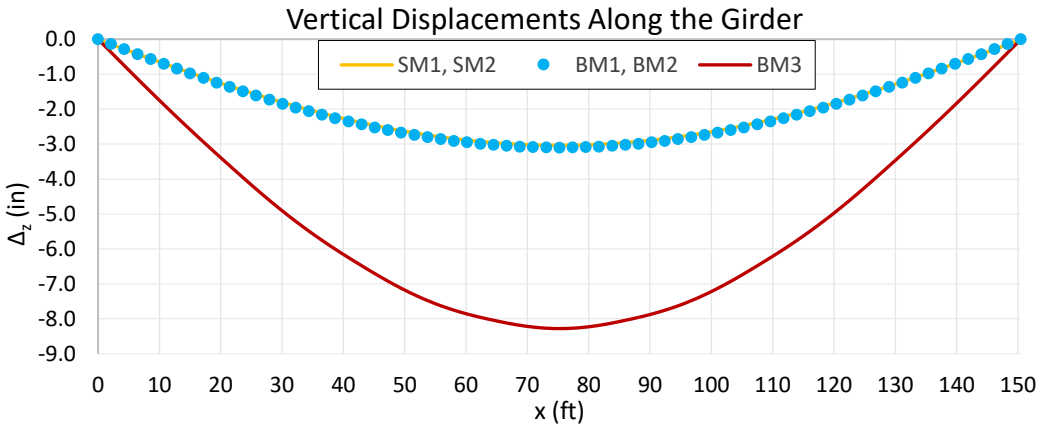

Figure 4-17 Vertical displacements along the girder.

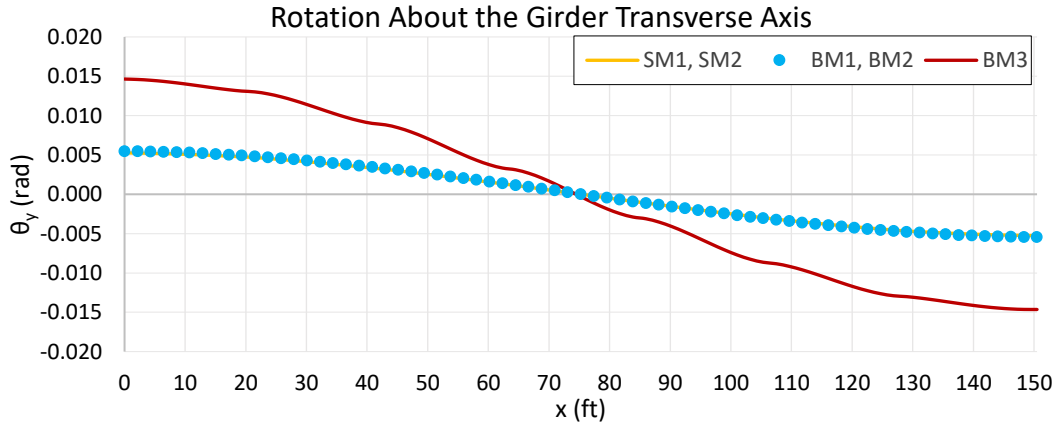

Figure 4-18 Rotation about the girder transverse axis.

As can be seen from the figures, neglecting the warping stiffness of the girder in the BM3 model causes a significant overestimation, almost 4 times larger vertical displacements at the center of the girder deflections. Thus, using conventional 6 DOF

beam elements to model curved I-beams under the bridge's self-weight would cause unrealistic cambering of such beams.

4.2.4 Twist angle

In contrast to beam models that do not take into account the web distortion and produce a single twist angle value at the centroid of the girder, the twist angle varies along the web depth in shell models. Since significant web distortions were observed within the unbraced segments of shell models, there is no comparison made between the shell and beam models of this case study in terms of the twist angle.

The plots of lateral displacement and twist angle along the web can be seen in Figure 4-19 for the middle of first and last unbraced segments, and for the mid-span.

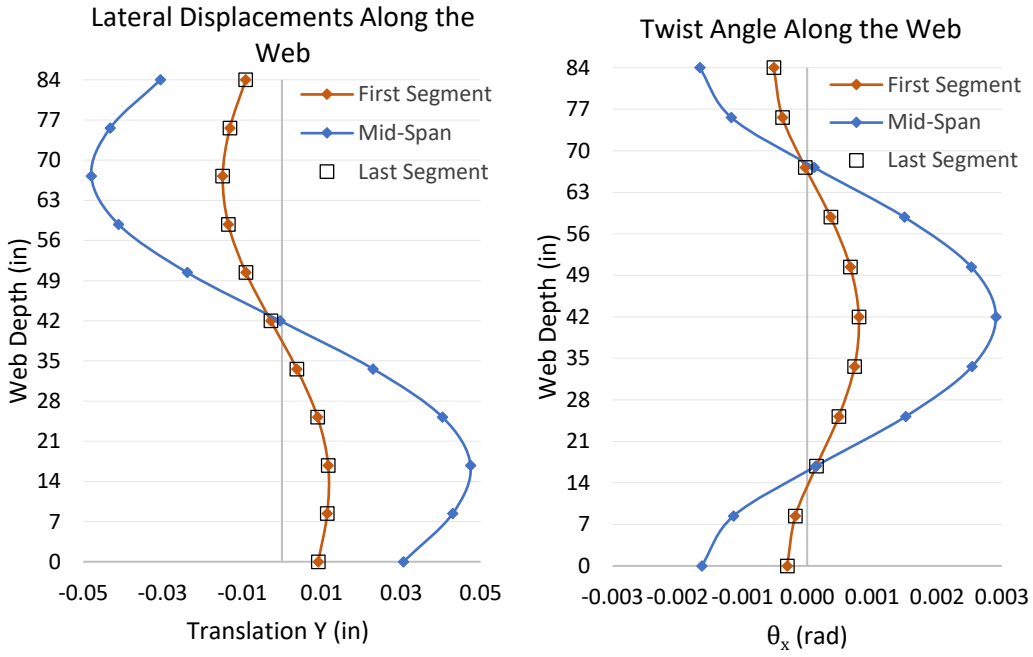

Figure 4-19 Lateral displacements and twist angle along the web.

4.2.5 Lateral bending

The lateral bending moments were extracted from the individual flanges of the girder from the shell models and reported separately for the top and bottom flange. The equal and opposite flange lateral bending moments were obtained by dividing the bi-moment output of the warping beam element by the distance between flange centroids. Additionally, the major-axis bending moment values obtained from the reference SM1 model were used in Equation 4-2, which is the approximate equation provided by AASHTO LRFD Bridge Design Specifications, and the lateral bending moment values due to curvature were calculated. (The constant N was taken as 12 in Equation 4-2.)

The results were plotted in Figure 4-20 and Figure 4-21. As can be seen from these figures, the warping beam model BM1 and the shell model SM2, which uses an alternative modeling approach for the flanges, are able to capture the response of the reference model, SM1. The approximate equation provides an upper bound for the flange lateral bending moments and captures the response of the reference model at the cross-frame locations. This is because the V-Load Method assumes the presence of a cross-frame at the point under consideration.

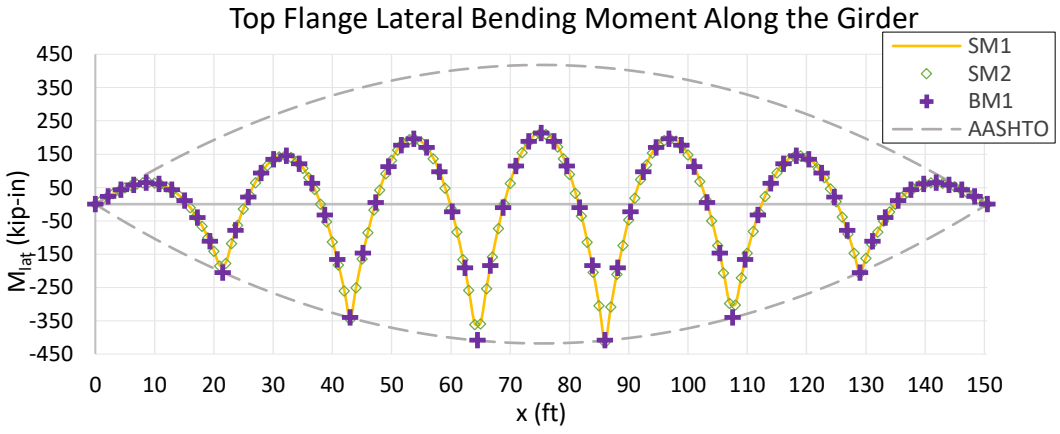

Figure 4-20 Top flange lateral bending moment along the girder.

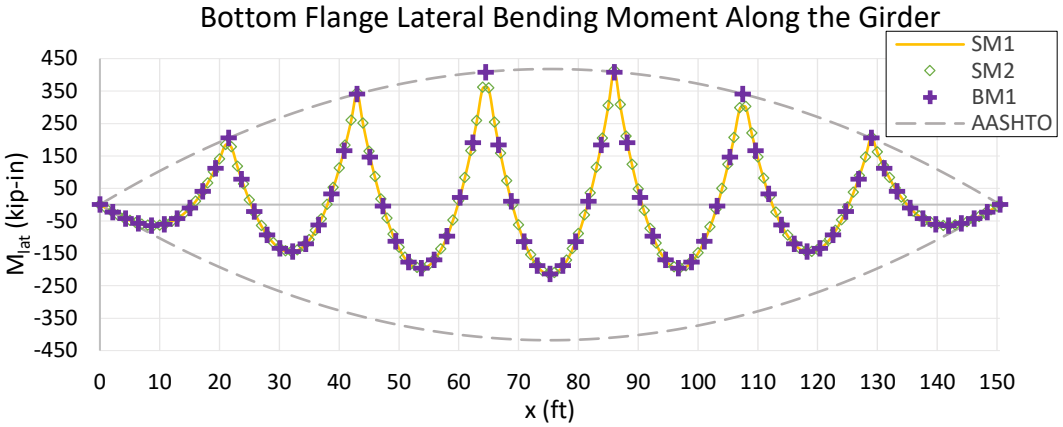

Figure 4-21 Bottom flange lateral bending moment along the girder.

4.2.6 Cross-frame forces

The equal and opposite lateral forces were obtained in the top and bottom chord of the cross-frames. The absence of a warping degree of freedom in the 6 DOF beam elements caused the cross-frame forces to differ from other analysis models as the warping boundary conditions could not be modeled accurately. Since the differences were negligible, the comparison of the results was not reported.

4.3 Case Study #3: Single Span Horizontally Curved I-Girder Bridge Under Deck Weight Loading

The bridge that is subject to this case study is a single span horizontally curved I-girder bridge, the dimensions of which are selected by taking the dimensions of the example bridge Bridge NISCR2, examined under Project NCHRP 12-79 (White et al., 2012), as a reference. The span length is 150.5 ft along the centerline, and the radius of curvature is 425 ft at the centerline. The cross-section of the bridge consists of four I-girders having the same cross-sectional and material properties which were used in the previous case study (Figure 4-14 and Table 4-5). The study bridge consists of the superstructure with idealized supports at the ends. The simple support conditions of the previous case study were utilized at the ends of each girder.

As shown in Figure 4-22, the uniform girder and cross-frame spacings are 8 ft and 21.5 ft, respectively. The cross-frames are full depth X-type cross-frame with top and bottom chords that can be seen through the 3D view of the bridge, in Figure 4-23.

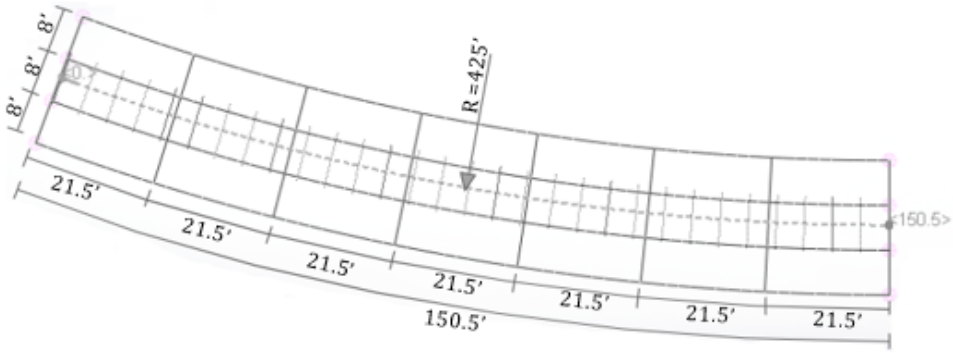

Figure 4-22 Plan view of the bridge.

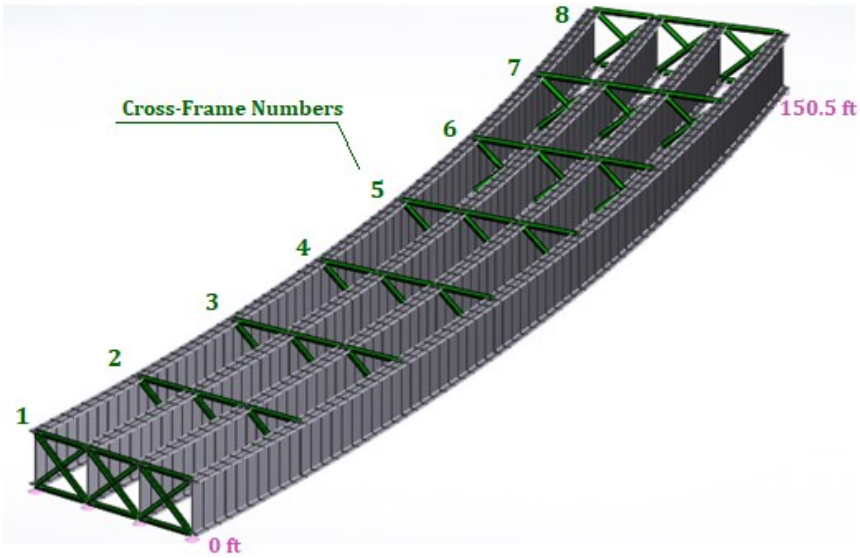

Figure 4-23 3D view of the bridge.

4.3.1 Deck weight loading

The bridge has 3 ft long overhang at both sides. The deck thickness, including integral wearing surface, was taken as 9.5 inches, and the unit weight of concrete used in the self-weight computation is 150 lb/ft^3. The deck weight acting on the interior and exterior girders were calculated as 950 lb/ft and 831.3 lb/ft, respectively.

In beam models, the loading was applied as uniform member loads. In shell models, the loading was applied as nodal loads on top of girders.

4.3.2 Analysis models

The sample bridge was modeled and analyzed in LARSA 4D finite element analysis software, also in 3D Frame Analysis Program following similar procedures as the previous case studies except that the cross-frames were modeled explicitly by truss elements and connected to nodes at the intersection of flanges and the web.

The dimensions of shell elements employed for the web and flanges in shell models, the number of elements employed for modeling girders in beam models, also the assumptions made regarding the warping conditions of the beam model with J_{eff} are same as the previous case study (Section 4.2.2). In beam models, the cross-frames were connected to the girder centroid through rigid connection members, which are 6 DOF conventional beam elements with large cross-sectional and material properties. Figure 4-24 shows the graphical illustration of these models with the corresponding elements.

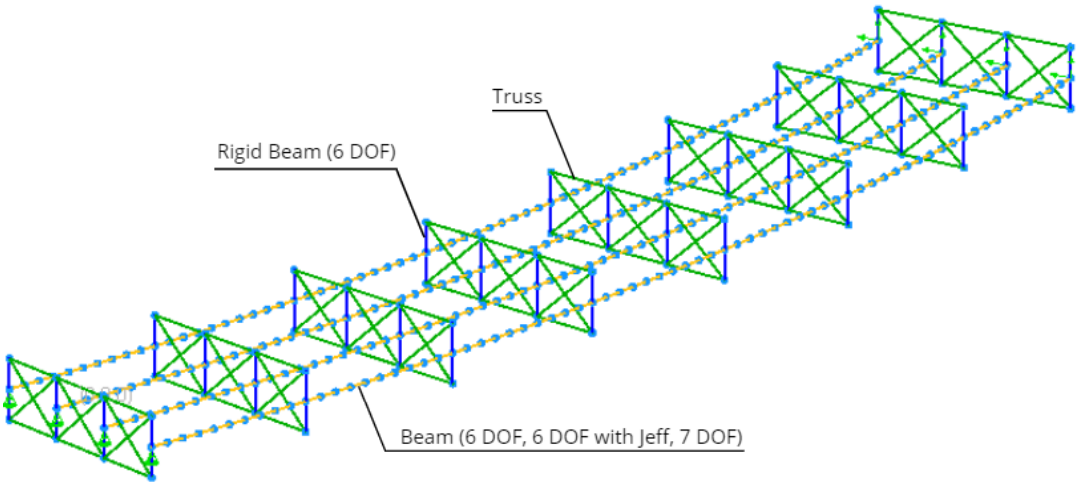

Figure 4-24 Beam models of the third case study.

All the analysis models of the present case study are summarized in Table 4-7.

Table 4-7 Analysis models of the third case study.

Analysis Models	
Shell Model 1 (SM1):	Girders are modeled as full-shell elements. Web distortion is prevented at cross-frame locations with rigid members.
Shell Model 2 (SM2):	The web is modeled as shell elements, flanges are modeled as beam elements. Web distortion is prevented at cross-frame locations with rigid members.
Beam Model 1 (BM1):	Girders are modeled as 7 DOF warping beam elements. Conventional 6 DOF rigid beams connect cross-frames and girders.
Beam Model 2 (BM2):	Girders are modeled as 6 DOF beam elements with J_{eff}. Conventional 6 DOF rigid beams connect cross-frames and girders.
Beam Model 3 (BM3):	Girders and rigid connection members between girders and cross-frames are modeled as conventional 6 DOF beam elements.

The SM1 model was taken as the reference model in comparisons. While reporting results, girders were numbered starting from the outside of the curve. The outermost girder corresponds to Girder 1, and the inside girder corresponds to Girder 4.

4.3.3 Major-axis bending

Similar to the previous case study, which analyzes an isolated curved girder, all analysis models produced similar results for the vertical displacements except the BM3 model with conventional 6 DOF beam elements. In Table 4-8, vertical displacements at the mid-span of girders were reported. As can be seen from the table, neglecting the warping stiffness of girders in the BM3 model causes the girder vertical deflections to be overestimated.

Table 4-8 Vertical displacements at the mid-span, in inches.

Girder	SM1	SM2	BM1	BM2	BM3
G1	-6.87	-6.87 (0.0%)	-6.82 (-0.7%)	-6.63 (-3.5%)	-18.42 (168.1%)
G2	-5.06	-5.06 (0.0%)	-5.03 (-0.6%)	-4.95 (-2.2%)	-13.63 (169.4%)
G3	-3.28	-3.27 (-0.3%)	-3.25 (-0.9%)	-3.30 (0.6%)	-8.85 (169.8%)
G4	-1.50	-1.50 (0.0%)	-1.49 (-0.7%)	-1.66 (10.7%)	-4.08 (172.0%)

Note: The values in brackets are percentage errors with reference to the SM1 model.

In addition to the vertical displacements, the major-axis bending moments were extracted from the analysis models, and the major-axis bending stresses were computed relative to the elastic neutral axis, which is at the girder centroid. The stress values at the mid-span of girders were reported in Table 4-9.

Table 4-9 Bottom flange major-axis bending stresses at the mid-span, in ksi.

Girder	SM1	SM2	BM1	BM2	BM3
G1	18.81	18.81 (0.0%)	18.80 (-0.1%)	17.8 (-5.4%)	18.63 (-1.0%)
G2	13.29	13.29 (0.0%)	13.29 (0.0%)	12.94 (-2.6%)	13.25 (-0.3%)
G3	7.41	7.41 (0.0%)	7.41 (0.0%)	7.73 (4.3%)	7.47 (0.8%)
G4	1.07	1.07 (0.0%)	1.07 (0.0%)	2.11 (97.2%)	1.22 (14.0%)

Note: The values in brackets are percentage errors with reference to the SM1 model.

As can be seen from the table, stresses obtained from the shell model, SM2, and warping beam model, BM1 was identical to the stresses obtained from the reference model. While the BM3 model produced erroneous results for the vertical displacements, it produced similar results for the major-axis bending stresses as the reference model, meaning that the major-axis bending stresses were not much affected by the warping contributions.

Regarding the BM2 model, the assumption of warping fixity at the intermediate cross-frame locations caused the bridge torsional stiffness to be overestimated as a system, and less load was transferred from the inner girders to the outside girder when compared with the results of the reference model. The effect of this assumption was not apparent in vertical displacements (Table 4-8), also in the major-axis bending stresses of Girder 1 to 3 (Table 4-9). However, the BM2 model overestimates the major-axis bending moments and stresses significantly for Girder 4, as shown in Figure 4-25 and Figure 4-26.

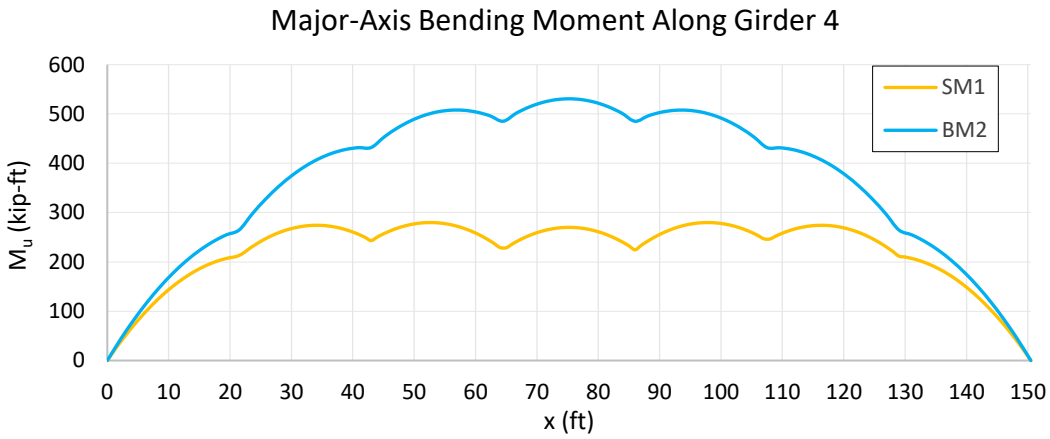

Figure 4-25 Major-axis bending moment along Girder 4.

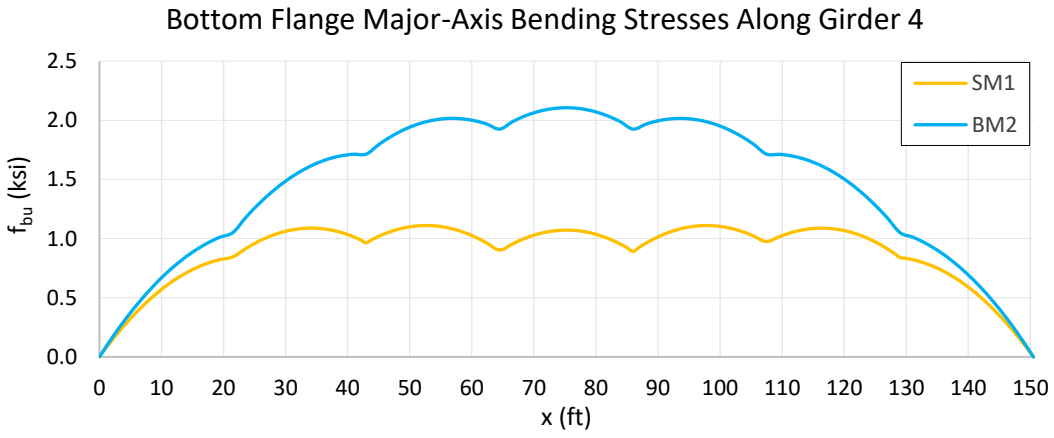

Figure 4-26 Bottom flange major-axis bending stresses along Girder 4.

4.3.4 Twist angle

Figure 4-27 and Figure 4-28 shows the comparison of the twist angles along exterior girders obtained from the BM3 model and the reference SM1 model. As seen in the figures, the twist angle values of the BM3 model are larger than the reference model as a consequence of neglecting the warping effects. The twist angle values at the mid-span of Girder 1 and Girder 4 are almost eleven times and three times greater than the reference model, respectively. The twist angle values obtained from all other analysis models were close to each other.

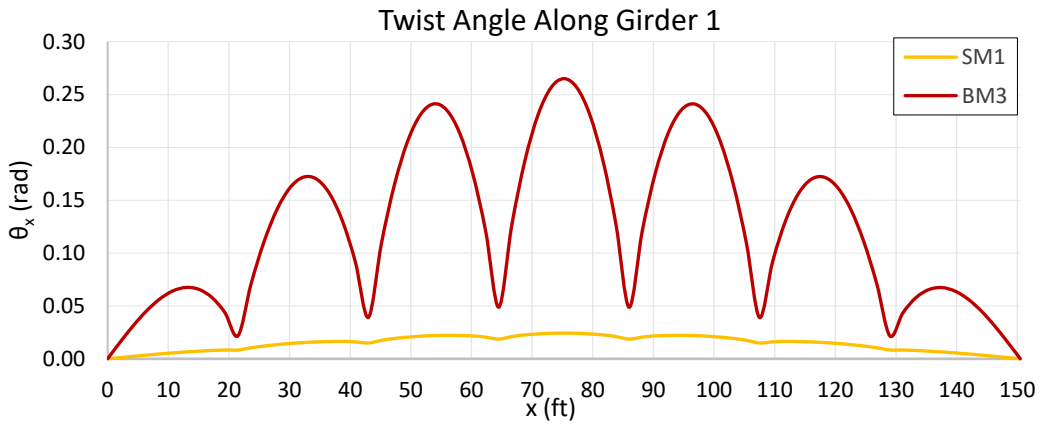

Figure 4-27 Twist angle along Girder 1 for models SM1 and BM3.

Figure 4-28 Twist angle along Girder 4 for models SM1 and BM3.

In Figure 4-29 and Figure 4-30, twist angle values along the exterior girders are plotted for BM1 and BM2 models together with the reference model. Since the SM1 and SM2 models produced identical results, they are grouped together.

The twist angle values within the unbraced length of shell models are larger than the warping beam model BM1 due to Vlasov's assumption of no web distortion during twisting. As the web distortion decreases from Girder 1 to Girder 4 (Figure 4-31), the results become closer.

Compared to the reference model, the BM2 model produces close results by approximating the torsional stiffness with the effective torsion constant, based on the assumption of warping fixity at the cross-frame locations.

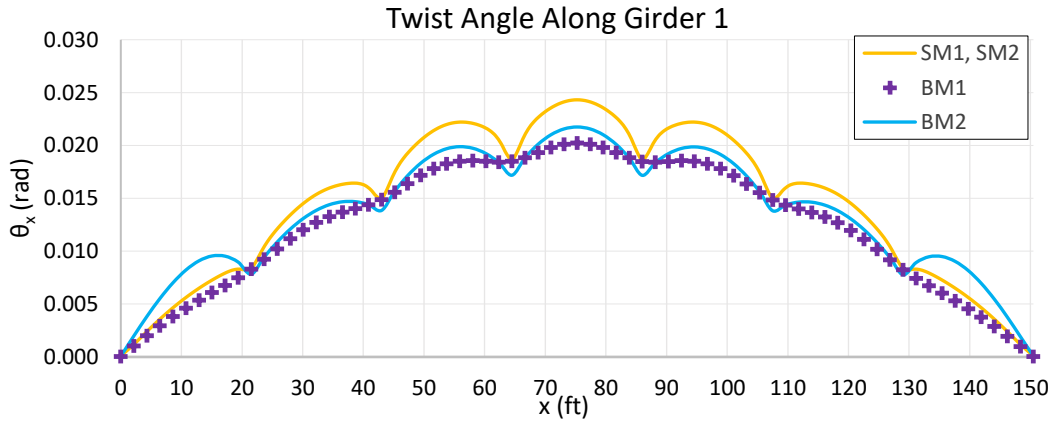

Figure 4-29 Twist angle along Girder 1 for models SM1, SM2, BM1, and BM2.

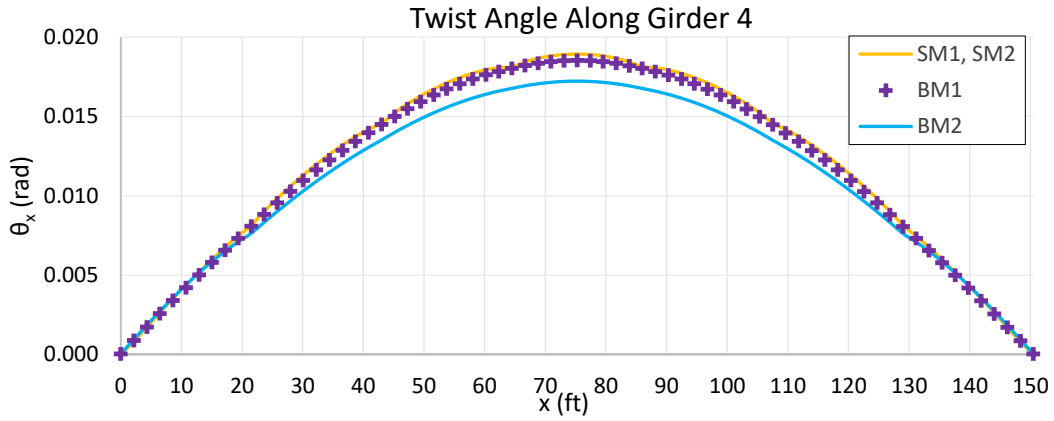

Figure 4-30 Twist angle along Girder 4 for models SM1, SM2, BM1, and BM2.

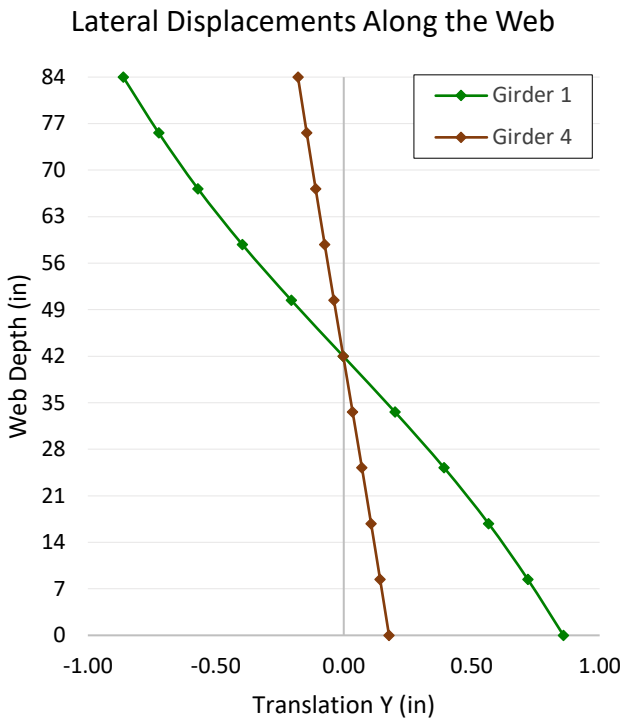

Figure 4-31 Lateral displacements along the web, at the mid-span of Girder 1 and Girder 4.

4.3.5 Lateral bending

The lateral bending moments were extracted from the individual flanges of shell models' girders. The equal and opposite flange lateral bending moments were obtained by dividing the bi-moment output of the warping beam element by the distance between the flange centroids. Additionally, the major-axis bending moment values obtained from the reference SM1 model were used in Equation 4-2, which is the approximate equation provided by AASHTO LRFD Bridge Design Specifications, and the lateral bending moment values due to curvature were calculated. (The constant N was taken as 12 in Equation 4-2.)

The obtained lateral bending moments were then divided by the section modulus of the flanges, and the lateral bending stresses were computed. For all girders, the

warping beam model BM1 and the shell model SM2, which uses an alternative modeling approach for the flanges, were able to capture the response of the reference model, SM1. For Girder 1 to Girder 3, the approximate equation produced conservative flange lateral bending stresses throughout the length of the girder; however, it produced unconservative results within the unbraced lengths of Girder 4. From Figure 4-32 to Figure 4-35, lateral bending stresses along Girder 2 and Girder 4 are plotted separately for the top and bottom flange.

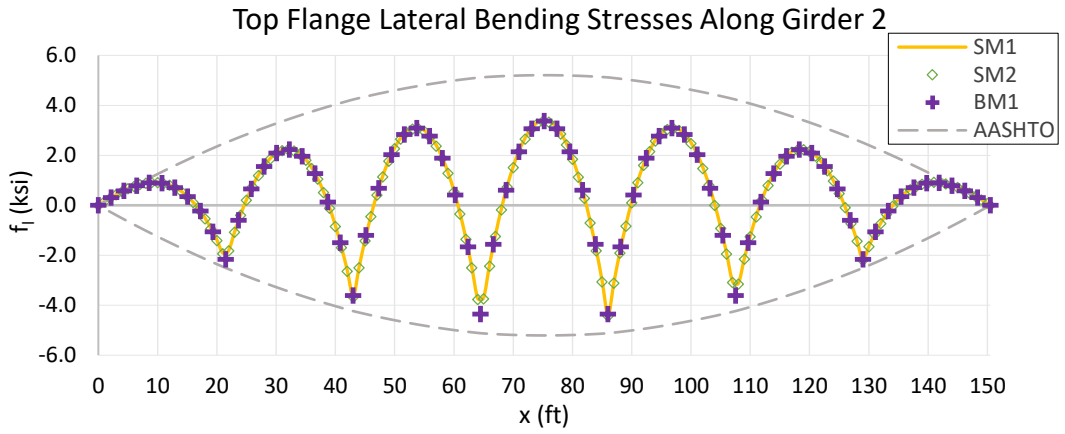

Figure 4-32 Top flange lateral bending stresses along Girder 2.

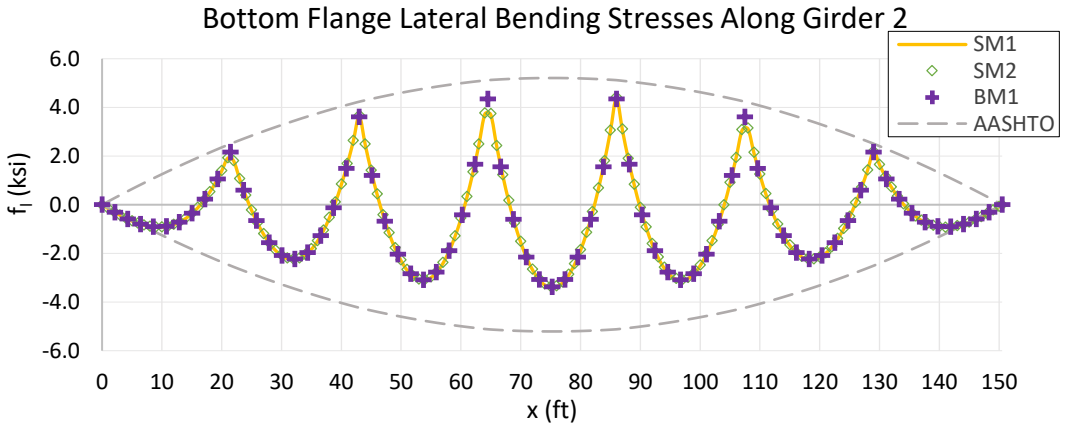

Figure 4-33 Bottom flange lateral bending stresses along Girder 2.

As seen in the figures, the approximate equation produced reasonable results at cross-frame locations as the V-Load Method assumes the presence of a cross-frame at the point under consideration. However, different from the previous case study, the results do not perfectly match with the other reported results at the cross-frame locations. As an example, the top flange lateral bending stress of Girder 2 produced by the approximate equation at the fifth cross-frame location, i.e., 86 ft, is 17% greater than the stress obtained from the reference model. The reason for that is the V-Load Method analyzes flange as a continuous beam rigidly supported at the cross-frame locations. Since the cross-frames were represented by lateral restraints in the previous case study, the approximate equation produced exact results at these locations. In the current case study, the cross-frames are explicitly modeled, and flanges are not rigidly supported at these locations. Therefore, the results obtained from the approximate equation show deviations at the cross frame locations, and the approximate equation produces unconservative results for Girder 4. At the mid-span of Girder 4, i.e., 75.25 ft, the top flange lateral bending stress produced by the approximate equation is 60% less than the stress obtained from the reference model.

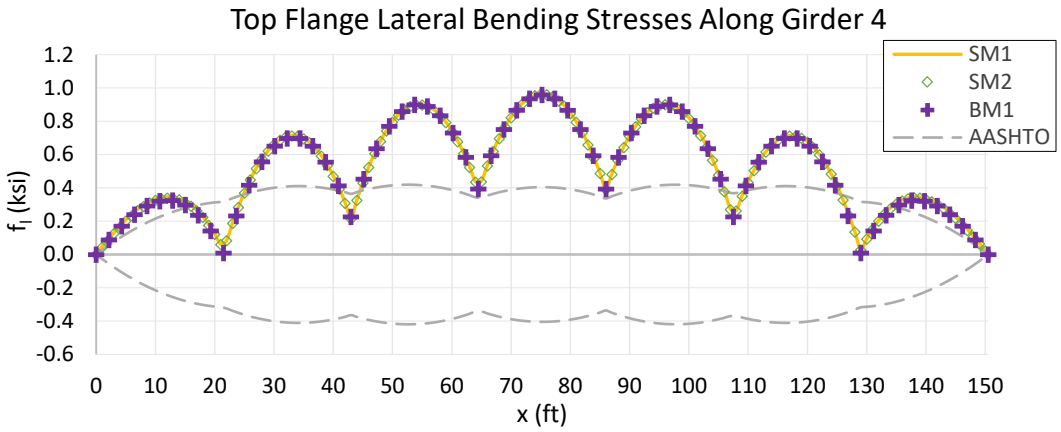

Figure 4-34 Top flange lateral bending stresses along Girder 4.

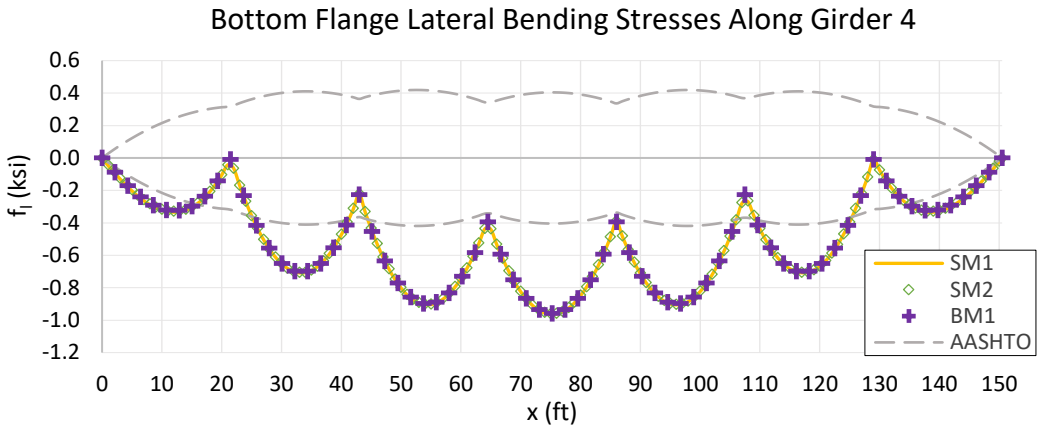

Figure 4-35 Bottom flange lateral bending stresses along Girder 4.

4.3.6 Support reactions and cross-frame forces

Under uniform deck weight loading, the reactions obtained at the start and end of girders were equal. In all analysis models, the distribution of reactions was similar, as shown in Table 4-10. Since the bridge is under torsional action due to its curved geometry, reactions are larger at the outer girder and smaller at the inner girder as expected.

Table 4-10 Vertical support reactions at the start and end of girders, in kips.

Girder	SM1	SM2	BM1	BM2	BM3
G1	114.1	114.1	112.5	113.3	113.1
G2	82.7	82.7	83.8	81.9	82.9
G3	51.2	51.3	54.0	55.2	53.9
G4	20.1	20.1	17.9	17.7	18.2

Note: The values are identical for the start and end of girders. Duplicates are not shown.

Regarding the cross-frame forces, discrepancies are observed between shell and beam models for the first and last cross-frames due to the difference in modeling

support conditions. For the intermediate cross-frames, all analysis models produced close results.

From Figure 4-36 to Figure 4-38, the axial forces in one of the diagonals were plotted for analysis models SM1, BM1, and BM2, relative to the cross frame numbers shown in Figure 4-23. There were slight differences between the results of SM1 and SM2 models, also between the results of BM1 and BM3 models. Since the differences were not visible in the graphs, the results of SM2 and BM3 models are not shown for clarity.

The cross-frame forces of the BM2 model deviate from the reference model as a result of the warping fixity assumption at the intermediate cross-frame locations.

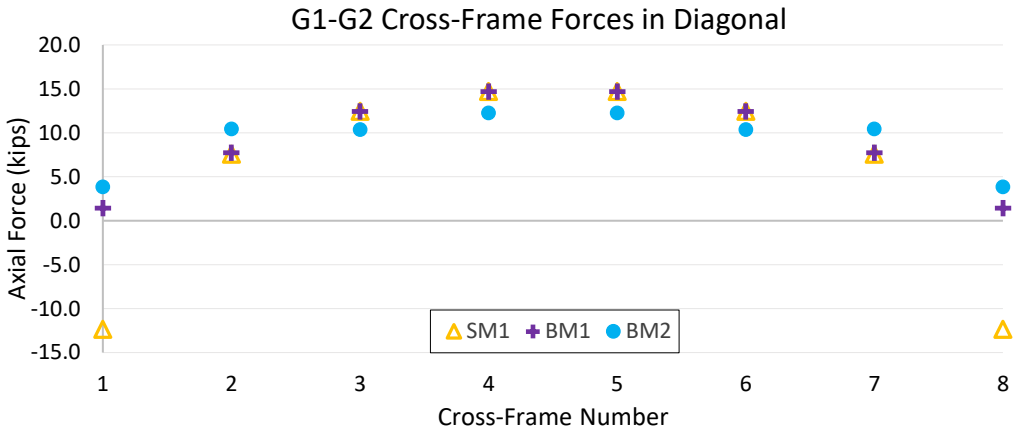

Figure 4-36 Forces in diagonal (between the top of G1 and the bottom of G2).

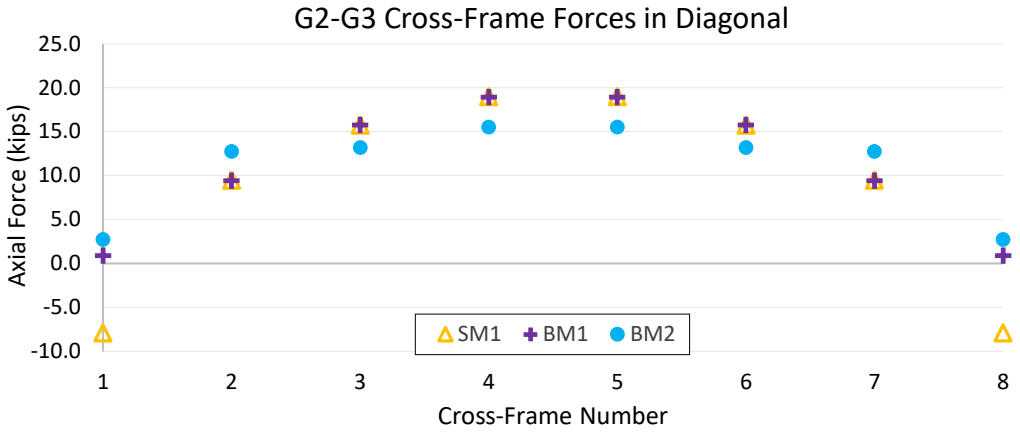

Figure 4-37 Forces in diagonal (between the top of G2 and the bottom of G3).

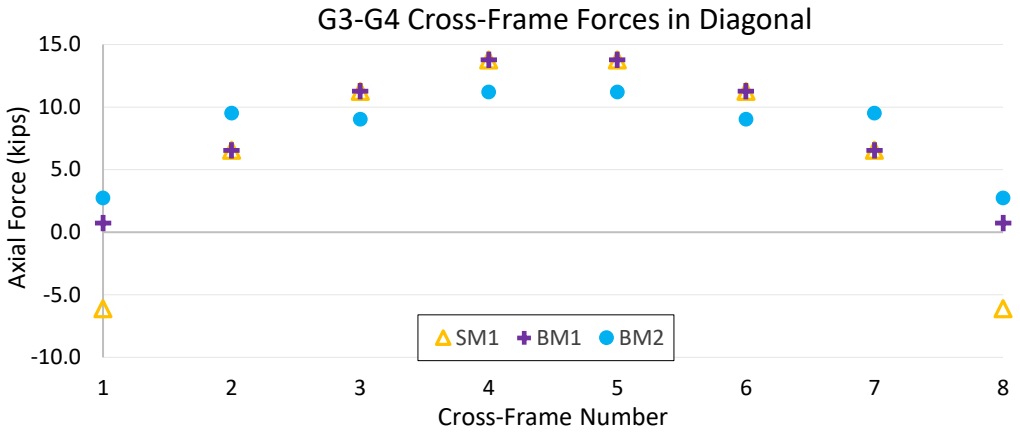

Figure 4-38 Forces in diagonal (between the top of G3 and the bottom of G4).

CHAPTER 5

SUMMARY AND CONCLUSIONS

In finite element analysis of steel I-girder bridges, the restrained warping behavior of girder can be considered through detailed 3D shell models or alternative methods such as utilizing an effective torsion constant in the analysis with conventional beam elements. For practical purposes, there is still a need for an intermediate modeling approach that is time-saving, reliable, and will provide specific analysis output parameters with sufficient accuracy.

In this study, a practical finite element modeling approach is investigated by utilizing 7 DOF beam elements that consider restrained warping behavior as an additional degree of freedom for girders. A comparative study was performed by assessing the results of various shell models and beam models, from the analysis and design aspects. The beam models of the study were analyzed in the 3D Frame Analysis Program, which was developed in MATLAB. The space truss element, 6 DOF conventional beam element, 6 DOF conventional beam element that uses an effective torsion constant (J_{eff}) to consider warping effects, and 7 DOF warping beam element were implemented into the program. The shell models of the study were analyzed in LARSA 4D program through thin-Drilling and thin-incompatible shell elements available in the program. In addition to full-shell finite element models in which multiple shell elements constitute the cross-section of the member, an alternative modeling approach is considered by modeling the web of the cross-section with shell elements and its flanges with beam elements.

Different modeling approaches were validated under torsional loading by comparing the analysis results with the analytical solution. The analytical solution for torsion and formulation of 7 DOF warping beam element was based on Vlasov's theory, which neglects shear deformation effects on warping and assumes that the web

remains straight during twisting. Since the I-section members have small torsional rigidity and exhibit large amounts of warping, also the girders having thin webs are generally provided with stiffeners, the assumptions of Vlasov's theory were considered admissible for practical purposes. The results obtained from beam models utilizing 7 DOF warping beam elements were capable of capturing the analytical solution for an I-section member under torsionally fixed-free and fixed-fixed boundary conditions. When multiple 6 DOF beam elements with J_{eff} were employed to model the member, larger twist angle values were obtained from the corresponding beam models compared to the analytical solution and other analysis models. While the variation of torsional moments and bi-moment obtained from analytical solution and shell models were similar, slight differences were observed in twist angle values. The differences were found to be mainly due to the no web distortion assumption of Vlasov's theory during twisting. In case the web distortion is prevented in shell models by means of rigid members, the twist angle values were also in line with the analytical solution. During the validation process, it was found out that the thin-drilling shell models show stiff behavior in the presence of rigid members.

Three case studies were conducted to understand to what extend the 7 DOF warping beam element can produce accurate analysis results and to qualify the usability of this element in the current bridge engineering practice. Case studies focused on the non-composite response of girders under construction loads and important design parameters such as major-axis and flange lateral bending stresses. The results of different modeling approaches were compared by taking the 3D full-shell model as a reference. In the analysis with J_{eff}, the warping was assumed to be free at the simply supported ends of the girder and restrained at cross-frame locations. There is no such assumption required in the analysis with 7 DOF warping beam elements. The conclusions drawn from these case studies are summarized in the following paragraphs.

For curved I-girders in which the bending and torsional actions are coupled, neglecting girder warping stiffness by using the 6 DOF conventional beam elements

in bridge superstructure modeling causes unrealistic cambering because the girder vertical deflections are significantly overestimated under the bridge's self-weight. In addition, this element overestimates the girder twist both for straight and curved I-girders. Therefore, the associated rotations should not be used to evaluate girder rotation limits or overhang vertical deflection limits given by the design specifications. Besides that, the element produced major-axis bending moments and cross-frame forces with sufficient accuracy for the example structures analyzed in this study.

When compared to the beam elements neglecting the girder warping stiffness, beam elements that incorporate the girder warping stiffness by means of an effective torsion constant provide a significant improvement in the analysis of steel I-girder bridges in terms of girder twist and vertical deflections. However, depending on the torsional stiffness of the bridge, the warping fixity assumed at the cross-frame locations to compute the effective torsion constant may yield incorrect analysis results for curved bridges. As in the case of the third case study, this assumption can cause the bridge torsional stiffness to be overestimated, and less load is transferred from the inner girders to the outside girder. As a result, the major-axis bending moments and stresses are overestimated for the inside girder.

The modeling approach, which uses the 7 DOF warping beam elements, and the alternative refined modeling approach, which uses the combination of shell-beam elements for steel I-girders, are both capable of producing all of the analysis output parameters considered in this study with sufficient accuracy. The only exception is that, since the 7 DOF warping beam elements neglect web distortion effects, this element can produce inaccurate twist angle results in cases where the web distortion is effective.

In conclusion, the modeling approach, which utilizes 7 DOF warping beam elements for steel I-girders, was found adequate in producing essential analysis output parameters with sufficient accuracy and can be used for practical purposes to consider the restrained warping behavior.

REFERENCES

Ahmed, M. Z., & Weisgerber, F. E. (1996). Torsion constant for matrix analysis of structures including warping effect. *International Journal of Solids and Structures*, *33*(3), 361–374.

American Association of State Highway and Transportation Officials. (2017). *AASHTO LRFD Bridge Design Specifications.* (8th ed.). Washington, D.C.

Ashiquzzaman, M., Hui, L., Schmeltz, J., Merino, C., Bozkurt, B., Ibrahim, A., … Hindi, R. (2016). *ICT PROJECT R27-140 Report: Effectiveness of Exterior Beam Rotation Prevention Systems for Bridge Deck Construction.*

Barsoum, R. S., & Gallagher, R. H. (1970). Finite element analysis of torsional and torsional–flexural stability problems. *International Journal for Numerical Methods in Engineering*, *2*(3), 335–352.

Batoz, J.-L., & Tahar, M. Ben. (1982). Evaluation of a new quadrilateral thin plate bending element. *International Journal for Numerical Methods in Engineering*, *18*(11), 1655–1677.

Benscoter, S. U. (1954). A theory of torsion bending for multicell beams. *Journal of Applied Mechanics*, *21*(1), 25–34.

Chang, C. J., & White, D. W. (2008). An assessment of modeling strategies for composite curved steel I-girder bridges. *Engineering Structures*, *30*(11), 2991–3002.

Cook, R. D., Malkus, D. S., Plesha, M. E., & Witt, R. J. (2001). *Concepts and Applications of Finite Element Analysis* (4th ed.). John Wiley & Sons.

Damkilde, L. (1999). *Elementmetodeformulering af tyndvæggede bjælker*.

Fiecht, A. L., Fenves, G. L., & Frank, K. H. (1987). *APPROXIMATE ANALYSIS OF HORIZONTALLY CURVED GIRDER BRIDGES* (Vol. 7).

Ibrahimbegovic, A., Taylor, R. L., & Wilson, E. L. (1990). A robust quadrilateral

membrane finite element with drilling degrees of freedom. *International Journal for Numerical Methods in Engineering*, *30*(3), 445–457.

Linzell, D. G., & Shura, J. F. (2010). Erection behavior and grillage model accuracy for a large radius curved bridge. *Journal of Constructional Steel Research*, *66*(3), 342–350.

Montoya-Vargas, S., & Dario Aristizabal-Ochoa, J. (2019). Torsion of prismatic I-beams with partially restrained warping at the end supports: Bending analogy method. *Engineering Structures*, *180*, 621–629.

Pezeshky, P. (2017). *Distortional Static and Buckling Analysis of Wide Flange Steel Beams*. University of Ottawa.

Salmon, C. G., Johnson, J. E., & Malhas, F. A. (2009). Steel Structures: Design and Behavior. *Structural Systems: Behaviour and Design*. Pearson/Prentice Hall.

Sanchez, T. A., & White, D. W. (2017). Improved 2D-Grid Construction Analysis of Curved and Skewed Steel I-Girder Bridges. *Journal of Bridge Engineering*, *22*(9), 1–11.

Seaburg, P. A., & Carter, C. J. (2003). Torsional Analysis of Structural Steel Members. In *AISC Steel Design Guide Series #9*. Chicago, IL: American Institute of Steel Construction.

Shakourzadeh, H., Guo, Y. Q., & Batoz, J. L. (1995). A torsion bending element for thin-walled beams with open and closed cross sections. *Computers and Structures*, *55*(6), 1045–1054.

Vlasov, V. Z. (1961). *Thin-Walled Elastic Beams*.

Waldron, P. (1986). Stiffness analysis of thin-walled girders. *Journal of Structural Engineering (United States)*, *112*(6), 1366–1384.

White, D. W., Coletti, D., Chavel, B. W., Sanchez, A., Ozgur, C., Chong, J. M. J., … Kowatch, G. T. (2012). *NCHRP Report 725 - Guidelines for Analysis*

Methods and Construction Engineering of Curved and Skewed Steel Girder Bridges.

Yang, Y., & McGuire, W. (1984). *A Procedure for Analysing Space Frames with Partial Warping Restraint*. *20*, 1377–1398.

Zhang, H., Huang, D., & Wang, T.-L. (2005). Lateral Load Distribution in Curved Steel I-Girder Bridges. *Journal of Bridge Engineering*, *10*(3), 281–290.

APPENDIX A - Element Stiffness Matrices

The stiffness matrix for Truss Element:

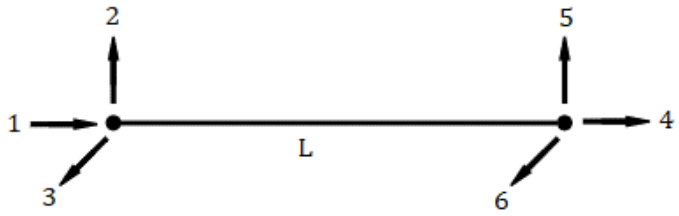

$$\frac{E}{L^3}\begin{bmatrix} AL^2 & 0 & 0 & -AL^2 & 0 & 0 \\ & 0 & 0 & 0 & 0 & 0 \\ & & 0 & 0 & 0 & 0 \\ Sym. & & & AL^2 & 0 & 0 \\ & & & & 0 & 0 \\ & & & & & 0 \end{bmatrix}$$

The stiffness matrix for 6 DOF Beam Element:

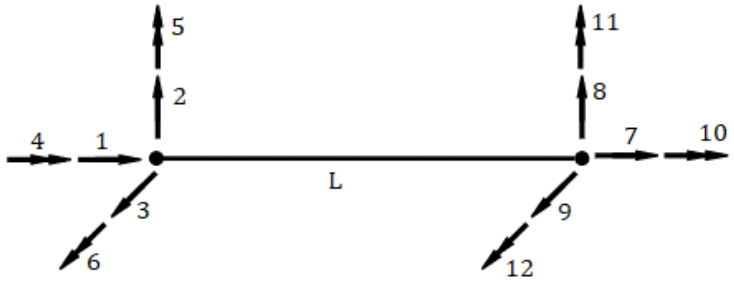

$$\frac{E}{L^3}\begin{bmatrix} k_1 & 0 & 0 & 0 & 0 & 0 & k_{1-7} & 0 & 0 & 0 & 0 & 0 \\ & k_2 & 0 & 0 & 0 & k_{2-6} & 0 & k_{2-8} & 0 & 0 & 0 & k_{2-12} \\ & & k_3 & 0 & k_{3-5} & 0 & 0 & 0 & k_{3-9} & 0 & k_{3-11} & 0 \\ & & & k_4 & 0 & 0 & 0 & 0 & 0 & k_{4-10} & 0 & 0 \\ & & & & k_5 & 0 & 0 & 0 & k_{5-9} & 0 & k_{5-11} & 0 \\ & & & & & k_6 & 0 & k_{6-8} & 0 & 0 & 0 & k_{6-12} \\ & & & & & & k_7 & 0 & 0 & 0 & 0 & 0 \\ & & & & & & & k_8 & 0 & 0 & 0 & k_{8-12} \\ & & & & & & & & k_9 & 0 & k_{9-11} & 0 \\ & & & & Sym. & & & & & k_{10} & 0 & 0 \\ & & & & & & & & & & k_{11} & 0 \\ & & & & & & & & & & & k_{12} \end{bmatrix}$$

$$k_1 = k_7 = -k_{1-7} = AL^2$$

$$k_2 = k_8 = -k_{2-8} = \frac{12I_z}{(1+\varphi_y)}$$

$$k_{2-6} = k_{2-12} = -k_{6-8} = -k_{8-12} = \frac{6LI_z}{(1+\varphi_y)}$$

$$k_3 = k_9 = -k_{3-9} = \frac{12I_y}{(1+\varphi_z)}$$

$$k_{3-5} = k_{3-11} = -k_{5-9} = -k_{9-11} = -\frac{6LI_y}{(1+\varphi_z)}$$

$$k_4 = k_{10} = -k_{4-10} = \frac{GJL^2}{E}$$

$$k_5 = k_{11} = \frac{(4+\varphi_z)L^2I_y}{(1+\varphi_z)}$$

$$k_{5-11} = \frac{(2-\varphi_z)L^2I_y}{(1+\varphi_z)}$$

$$k_6 = k_{12} = \frac{(4+\varphi_y)L^2I_z}{(1+\varphi_y)}$$

$$k_{6-12} = \frac{(2-\varphi_y)L^2I_z}{(1+\varphi_y)}$$

The stiffness matrix for 7 DOF Warping Beam Element:

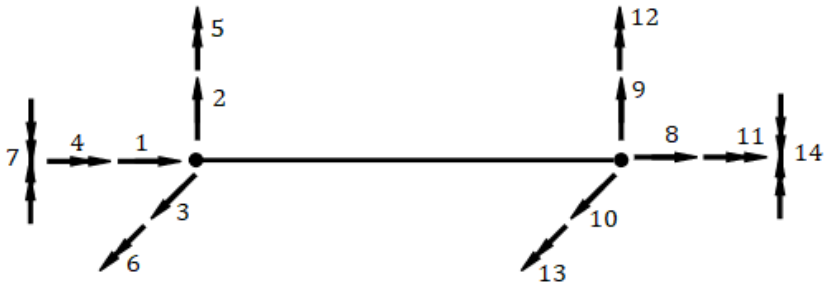

$$\frac{E}{L^3}\begin{bmatrix} k_1 & 0 & 0 & 0 & 0 & 0 & 0 & k_{1-8} & 0 & 0 & 0 & 0 & 0 & 0 \\ & k_2 & 0 & 0 & 0 & k_{2-6} & 0 & 0 & k_{2-9} & 0 & 0 & 0 & k_{2-12} & 0 \\ & & k_3 & 0 & k_{3-5} & 0 & 0 & 0 & 0 & k_{3-10} & 0 & k_{3-12} & 0 & 0 \\ & & & k_4 & 0 & 0 & k_{4-7} & 0 & 0 & 0 & k_{4-11} & 0 & 0 & k_{4-14} \\ & & & & k_5 & 0 & 0 & 0 & 0 & k_{5-10} & 0 & k_{5-12} & 0 & 0 \\ & & & & & k_6 & 0 & 0 & k_{6-9} & 0 & 0 & 0 & k_{6-12} & 0 \\ & & & & & & k_7 & 0 & 0 & 0 & k_{7-11} & 0 & 0 & k_{7-14} \\ & & & & & & & k_8 & 0 & 0 & 0 & 0 & 0 & 0 \\ & & & & & & & & k_9 & 0 & 0 & 0 & k_{9-13} & 0 \\ & & & & Sym. & & & & & k_{10} & 0 & k_{10-12} & 0 & 0 \\ & & & & & & & & & & k_{11} & 0 & 0 & k_{11-14} \\ & & & & & & & & & & & k_{12} & 0 & 0 \\ & & & & & & & & & & & & k_{13} & 0 \\ & & & & & & & & & & & & & k_{14} \end{bmatrix}$$

$$k_1 = k_8 = -k_{1-8} = AL^2$$

$$k_2 = k_9 = -k_{2-9} = \frac{12I_z}{(1+\varphi_y)}$$

$$k_{2-6} = k_{2-13} = -k_{6-9} = -k_{9-13} = \frac{6LI_z}{(1+\varphi_y)}$$

$$k_3 = k_{10} = -k_{3-10} = \frac{12I_y}{(1+\varphi_z)}$$

$$k_{3-5} = k_{3-12} = -k_{5-10} = -k_{10-12} = -\frac{6LI_y}{(1+\varphi_z)}$$

$$k_4 = k_{11} = -k_{4-11} = \frac{6GJL^2}{5E} + 12C_w$$

$$k_{4-7} = k_{4-14} = -k_{7-11} = -k_{11-14} = \frac{GJL^3}{10E} + 6C_wL$$

$$k_5 = k_{12} = \frac{(4+\varphi_z)L^2I_y}{(1+\varphi_z)}$$

$$k_{5-12} = \frac{(2-\varphi_z)L^2I_y}{(1+\varphi_z)}$$

$$k_6 = k_{13} = \frac{(4+\varphi_y)L^2I_z}{(1+\varphi_y)}$$

$$k_{6-13} = \frac{(2-\varphi_y)L^2I_z}{(1+\varphi_y)}$$

$$k_7 = k_{14} = \frac{2GJL^4}{15E} + 4C_wL^2$$

$$k_{7-14} = -\frac{GJL^4}{30E} + 2C_wL^2$$

Where;

$$\varphi_y = \frac{12EI_z}{GA_yL^2}$$

$$\varphi_z = \frac{12EI_y}{GA_zL^2}$$

L: element length, E: modulus of elasticity, G: shear modulus, J: torsion constant, C_w: warping constant,

A: cross-sectional area, I_z: the moment of inertia about member local z-axis, I_y: the moment of inertia about member local y-axis, A_y: shear area in member local y-axis, and A_z: shear area in member local z-axis.

All stiffness matrices are symmetric.

APPENDIX B - Inputs and Outputs of the 3D Frame Analysis Program

Inputs of the Program

The inputs of the program are entered either relative to the local coordinate system of elements or the global coordinate system. The local coordinate system of an element is defined such that the x-axis of element directed along the member's centroidal axis from the start of the member to the end. For a horizontal member lying on the global X-axis, the member local-y and local-z axes coincide with the system global-Y and global-Z axes, respectively.

Input Spreadsheet: Properties

Property ID	E (ksi)	G (ksi)	A (in^2)	Iz (in^4)	Iy (in^4)	Shear Area in y (in^2)	Shear Area in z (in^2)	J (in^4)	Cw (in^6)

Properties: The input sheet for the material and cross-sectional properties. The material properties include modulus of elasticity (E), shear modulus (G), torsion constant (J), and warping constant (C_w). The cross-sectional properties include the section area (A), moments of inertia about member local z- and y- axes (I_z and I_y, respectively), the shear areas for transverse shear. All properties are entered in member local axes.

Input Spreadsheet: Nodes

Node ID	X Coordinate (in)	Y Coordinate (in)	Z Coordinate (in)

Nodes: The input sheet for the coordinates of element nodes, in other words, for the joint locations. The locations are entered as x-, y- and z-coordinates in the global coordinate system.

Input Spreadsheet: Elements

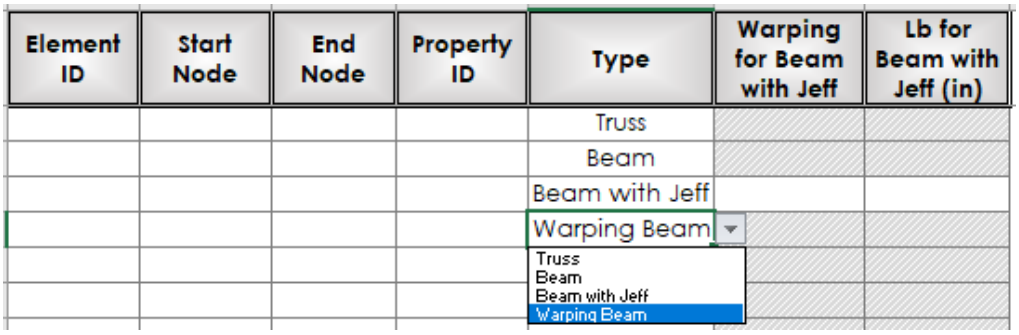

Elements: The input sheet for the element properties. These properties include connectivity of members defined by the start and end nodes of the element, the material and cross-sectional properties specified by the ID of property entered into *Properties* sheet, the type of element which can be one of *Truss*, *Beam*, *Beam with* J_{eff}, *Warping Beam*. Two properties for warping boundary conditions and unbraced length are only applicable to elements with type *Beam with* J_{eff}. Warping boundary conditions can be one of *Fixed-Fixed* and *Fixed-Free*. For intermediate elements defined between these boundaries, the two inputs should be the same. The unbraced length corresponds to the distance between warping boundaries.

Input Spreadsheet: Restraints

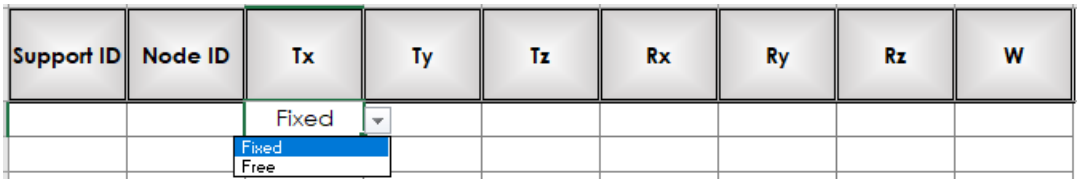

Restraints: The input sheet for the restraints or support conditions. The support conditions are specified as *Fixed* or *Free* for the available seven degrees of freedom with respect to the global coordinate system. The corresponding degrees of freedom are translation and rotation in x, y, z directions, and the warping DOF.

Input Spreadsheet: Nodal Loads

Load ID	Node ID	Fx (kips)	Fy (kips)	Fz (kips)	Mx (kips-in)	My (kips-in)	Mz (kips-in)	B ($kips\text{-}in^2$)

Nodal Loads: The input sheet for concentrated loads to be applied to nodes of the analysis model. The loads are specified with respect to the global coordinate system. The loads corresponding to the available degrees of freedom are translational forces and moments in x, y, z directions, and bi-moment.

Input Spreadsheet: Member Loads

Load ID	Member ID	Uniform Load in Local z (kips/in)	Uniform Torsion in Local x (kips-in/in)

Member Loads: The input sheet for uniformly distributed loads to be applied to members of the analysis model. The loads are assumed to act on the member centroidal axis and specified with respect to member local axes. The member loads available in the program are uniform load in member local-z direction and uniform torsion in member local-x direction.

Outputs of the Program

Output Spreadsheet: Joint Displacements

Joint	Tx (in)	Ty (in)	Tz (in)	Rx (rad)	Ry (rad)	Rz (rad)	W (rad/in)

Joint Displacements: The output sheet that reports joint displacements in global coordinates.

Output Spreadsheet: Member End Displacements

START NODE							END NODE						
Tx (in)	Ty (in)	Tz (in)	Rx (rad)	Ry (rad)	Rz (rad)	W (rad/in)	Tx (in)	Ty (in)	Tz (in)	Rx (rad)	Ry (rad)	Rz (rad)	W (rad/in)

Member End Displacements: The output sheet that reports element end displacements in element local coordinates.

Output Spreadsheet: Member End Forces

START NODE							END NODE						
Fx (kips)	Fy (kips)	Fz (kips)	Mx (kips-in)	My (kips-in)	Mz (kips-in)	B ($kips\text{-}in^2$)	Fx (kips)	Fy (kips)	Fz (kips)	Mx (kips-in)	My (kips-in)	Mz (kips-in)	B ($kips\text{-}in^2$)

Member End Forces (Local/Global): Two output sheets reporting element end forces in element local coordinates and global coordinates.

Output Spreadsheet: Support Reactions

Joint	Fx (kips)	Fy (kips)	Fz (kips)	Mx (kips-in)	My (kips-in)	Mz (kips-in)	B (kips-in2)

Support Reactions: The output sheet that reports support reactions at the restrained DOFs, in global coordinates.